Title

Organismal Benefits of Transcription Speed Control at Gene Boundaries

Xueyuan Leng[1], Maxim Ivanov[1], Peter Kindgren[1], Indranil Malik[2,6], Axel Thieffry[3,4], Peter Brodersen[4], Albin Sandelin[3,4], Craig D. Kaplan[2,5] and Sebastian Marquardt[1*].

[1] University of Copenhagen, Department of Plant and Environmental Sciences, Copenhagen Plant Science Centre, Frederiksberg, 1871 Denmark.
[2] Department of Biochemistry and Biophysics, Texas A&M University, College Station, Texas, 77843, United States.
[3] Biotech Research and Innovation Centre, University of Copenhagen, Copenhagen, 2200, Denmark.
[4] Department of Biology, University of Copenhagen, Copenhagen, 2200, Denmark.
[5] Department of Biological Sciences, University of Pittsburgh, Pittsburgh, Pennsylvania, 15260, United States.
[6] Current Address: Department of Neurology, University of Michigan Medical School, Ann Arbor, Michigan, MI 48109, United States

[*]Corresponding author
Correspondence: sebastian.marquardt@plen.ku.dk

Abstract

RNA polymerase II (RNAPII) transcription is crucial for gene expression. RNAPII density peaks at gene boundaries, associating these key regions for gene expression control with limited RNAPII movement. The connections between RNAPII transcription speed and gene regulation in multicellular organisms are poorly understood. Here, we directly modulate RNAPII transcription speed by point mutations in the second largest subunit of RNAPII in *Arabidopsis*

thaliana. A RNAPII mutation predicted to decelerate transcription is inviable, while accelerating RNAPII transcription confers phenotypes resembling auto-immunity. Nascent transcription profiling revealed that RNAPII complexes with accelerated transcription clear stalling sites at both gene ends, resulting in read-through transcription. The accelerated transcription mutant NRPB2-Y732F exhibits increased association with 5' splice site (5'SS) intermediates and enhanced splicing efficiency. Our findings highlight potential advantages of RNAPII stalling through local reduction of transcription speed to optimize gene expression for the development of multicellular organisms.

Introduction

A decisive step during gene expression is the conversion of the DNA sequences of a gene into pre-mRNA by RNA polymerase II (RNAPII) transcription. Profiles of RNAPII transcription across genes in eukaryotes revealed two main RNAPII localization peaks at gene boundaries, near gene transcription start sites (TSSs) and poly-adenylation sites (PASs) [1]. At the 3' end of genes, RNAPII peaks promote nascent RNA 3' end processing and transcriptional termination in mammals [2, 3]. The function of RNAPII peaks at promoter-proximal regions near TSSs is actively debated. On the one hand, "pause-release" of RNAPII can facilitate rapid induction of gene expression [4]; on the other hand, imaging of *Drosophila* and human RNAPII at promoter-proximal positions revealed rapid turnover, arguing against stable "pausing" of the same population of RNAPII complexes over time [5, 6]. In metazoans, the Negative Elongation Factor (NELF) complex promotes promoter proximal pausing of RNAPII by limiting RNAPII mobility [7]. However, NELF is conspicuously absent in yeast and plants, which implies that many organisms use alternative mechanisms to stall RNAPII at promoter proximal region (i.e. RNAPII stalling)[8]. In gene bodies, RNAPII accumulates at exon-intron boundaries and exhibits distinct accumulation profiles for exons with alternative splicing (AS) outcomes [9, 10]. The efficiency of splicing may hence be coupled to the local speed of RNAPII elongation at exon-intron boundaries [11]. In summary, peaks of accumulated RNAPII represent sites with low RNAPII forward movement, which may facilitate the integration of cellular signals to control gene expression post-initiation by co-transcriptional RNA processing [12].

RNAPII forward movement depends on the dynamics of the trigger loop (TL), a central structure in the RNAPII active center [13-15]. In addition, RNAPII backtracking induced by weak RNA-DNA hybrids (i.e. nucleotide misincorporation) limits RNAPII forward movement [16-18]. A “gating tyrosine” in the RNAPII second largest subunit RPB2 (i.e. Y769 in budding yeast Rpb2) stacks with the first backtracked nucleotide and is proposed to prevent further backtracking [19] and is also positioned to interact with the TL when in its closed, catalysis-promoting state. Point mutations in budding yeast Rpb1 TL residues and Rpb2 TL-interacting residues alter the RNAPII elongation speed *in vivo* [20-24]. Such “kinetic RNAPII mutants” have informed greatly on the effects of altered transcription speed on gene expression and transcription related phenotypes. For example, the budding yeast *rpb2-P1018S* slow transcription mutant (i.e. *rpb2-10*) promotes RNAPII arrest and reduces transcription processivity [25, 26]. Moreover, kinetic RNAPII mutants displaying accelerated transcription favor the use of upstream TSSs, while mutants displaying slow transcription tend to use downstream TSSs [27]. Variations of transcription speed alter profiles of co-transcriptional chromatin signatures and of RNAPII C-terminal domain (CTD) phosphorylation that impact pre-mRNA processing [28-30]. These observations indicate a profound effect of RNAPII transcription elongation speed on gene expression. The important question of whether growth and differentiation programs in a multi-cellular organism can be executed when RNAPII carries kinetic point mutations remains largely unclear.

Here, we altered RNAPII transcription activity in *Arabidopsis* through point mutations in NRPB2, the second largest subunit of *Arabidopsis* RNAPII. A mutant accelerating RNAPII transcription triggered phenotypes consistent with auto-immunity, but was able to execute key steps of pattern formation and organogenesis. A mutation predicted to decrease RNAPII transcription speed was inviable. Nascent RNAPII transcription profiling revealed that the mutant accelerating transcription resulted in reduced RNAPII stalling at both gene boundaries. Our findings highlight mechanistic connections between the intrinsic speed of RNAPII and RNAPII stalling at both gene boundaries that coordinate gene expression in the context of a multi-cellular organism.

Results

Altering transcription activity of RNAPII by targeted mutagenesis of NRPB2

To alter the *in vivo* RNAPII transcription activity in whole plants, we generated point mutations in *Arabidopsis* RNAPII. The target residues were identified in Rpb2, the second largest budding yeast RNAPII subunit. The Rpb2 proline 1018 to serine substitution (*rpb2-P1018S*) represents the classic slow transcription mutant *rpb2-10* and the tyrosine 769 to phenylalanine substitution (*rpb2-Y769F*) represents a mutation which might influence backtracking and trigger loop (TL) function (Fig 1A) [19, 31, 32]. Sequence alignments identified P979S and Y732F in the highly conserved regions of NRPB2, the second largest subunit of *Arabidopsis* RNAPII as the equivalent positions to budding yeast P1018S (*rpb2-10*) and Y769F respectively (Fig 1B). We generated these point mutations in constructs carrying the genomic *NRPB2* sequence fused to a C-terminal FLAG-tag driven by the endogenous *NRPB2* promoter and integrated them into the *nrpb2-2* null mutant background [33] (Fig EV1A). To investigate if these point mutations affected NRPB2 protein accumulation, we performed western blotting on FLAG-tagged $NRPB2_{P979S}$-FLAG, $NRPB2_{Y732F}$-FLAG and wild-type NRPB2-FLAG ($NRPB2_{WT}$-FLAG) (Fig 1C). We identified several individual transformant lines with comparable steady-state protein levels, thus any differences we detected in the characterization of these lines would have to be attributed to the effects of the point mutations on RNAPII activity.

The *Arabidopsis nrpb2-2* null-allele is female gametophytic lethal, but can be transmitted through the male germline with reduced transmission rate [33]. We could hence assay complementation of the gametophytic phenotypes to gain insights into the effects of RNAPII mutants. We assayed the transmission rate of the *nrpb2-2* null allele in the plants carrying homozygous $NRPB2_{WT}$, $NRPB2_{P979S}$ or $NRPB2_{Y732F}$ transgenes in *nrpb2-2 +/-* background (Fig EV1A). We would predict increased transmission rate of the *nrpb2-2* allele if the gametophytic defects could be complemented. As predicted, $NRPB2_{WT}$ can fully (i.e. to the expected level of 50%) complement the transmission of *nrpb2-2* compared to non-transformed controls (Fig 1D). Interestingly, $NRPB2_{Y732F}$ could almost fully complement *nrpb2-2* transmission, while $NRPB2_{P979S}$ did not significantly increase transmission rate compared to non-transformed controls (Fig 1D). These data suggest that $NRPB2_{P979S}$ fails to provide the RNAPII activity necessary for germline development. Indeed, silique dissection revealed that the germline defects in $NRPB2_{P979S}$ *nrpb2-2 +/-* were associated with reduced fertility and ovule abortion (Fig EV1B, C and D). Consistently, we identified plants homozygous for both $NRPB2_{Y732F}$ transgene and *nrpb2-2* mutant ($NRPB2_{Y732F}$ *+/+ nrpb2-2 -/-*) while $NRPB2_{P979S}$ *+/+*

nrpb2-2 -/- genotype could not be recovered. Remarkably, when all RNAPII complexes carried the $NRPB2_{Y732F}$ mutation (i.e. $NRPB2_{Y732F}$ +/+ *nrpb2-2 -/-*) we observed viable plant growth and development. These plants exhibited a dwarfed stature (Fig 1E and Fig EV1E), but resembled *Arabidopsis* seedlings concerning basic patterning and organ formation. The dwarfed stature was reminiscent of mutants displaying autoimmunity, which is often associated with increased expression of pathogen related (PR) genes [34]. Indeed, we detected elevated expression of *PR1*, *PR2* and *PR5* in $NRPB2_{Y732F}$ +/+ *nrpb2*-2 -/- compared to $NRPB2_{WT}$ +/+ *nrpb2*-2 -/- (Fig EV1F). These data highlight important roles of the ability to control the speed of RNAPII transcription during plant growth and development. In summary, *Arabidopsis* RNAPII harboring the $NRPB2_{P979S}$ point mutation failed to provide viable RNAPII activity during gametogenesis. However, the $NRPB2_{Y732F}$ mutation can partly rescue the germline defects in *nrpb2-2* null mutants and allow plant growth and basic aspects of development.

$NRPB2_{Y732F}$ accelerates RNAPII transcription *in vivo*

To investigate the effect of $NRPB2_{Y732F}$ on RNAPII transcription speed, we first tested if the equivalent *rpb2-Y769F* mutant in budding yeast classifies as a fast or slow RNAPII transcription mutant by assaying its sensitivity towards mycophenolic acid (MPA) and Mn^{2+} [35, 36]. Budding yeast RNAPII mutants conferring enhanced catalytic activity (RNAPII fast mutants) are more sensitive towards Mn^{2+} than the RNAPII slow mutants [20]. In budding yeast, RNAPII fast mutants are sensitive to MPA due to deficient expression of *IMD2* gene, which counteracts the inhibition of GTP synthesis by MPA. RNAPII slow mutants tend to be resistant to MPA due to the constitutive *IMD2* expression [21]. *rpb2-Y769F* exhibited strong growth defects towards MPA and Mn^{2+} while we observed no effect for *rpb2-P1018S* (Fig EV2A). *rpb2-Y769F* thus shows a growth phenotype consistent with fast RNAPII transcription mutants [20]. Interestingly, the *rpb2-Y769F*/*P1018S* double mutant exhibited mild sensitivity towards MPA compared to either single mutant (Fig EV2A), consistent with a complementary effect on transcription speed as seen across many RNAPII active site mutations in budding yeast [27]. Primer extension analyses of alternative TSSs usage of the *ADH1* gene represent an additional assay for RNAPII catalytic rate and therefore putative elongation speed [27], where catalytically hyperactive RNAPII mutants exhibit an upstream shift of TSS. In agreement with previously characterized fast RNAPII transcription mutants, *rpb2-Y769F* shifts the *ADH1* TSS

upstream compared to wild type or other Y769 substitutions (Fig EV2B). We next tested the combinations of *rpb2-Y769F* with trigger loop residue mutants previously demonstrated to alter RNAPII transcription speed. *rpb2-Y769F* was synthetically lethal with previously characterized fast RNAPII transcription mutants such as *rpb1-L1101S*, *rpb1-E1103G* and *rpb1-G1097D* (Fig EV2C), suggesting that these combinations synergistically accelerated RNAPII transcription and supporting the interaction between Y769 and TL-residues. Conversely, *rpb2-Y769F* suppressed the growth defect of previously characterized slow RNAPII transcription mutants such as *rpb1-F1086S*, *rpb1-H1085Q* and *rpb1-H1085Y* [27, 35] (Fig EV2C), suggesting compensatory effects on transcription speed when combining these "slow" mutations with *rpb2-Y769F*. In conclusion, our results characterized budding yeast *rpb2-Y769F* as a mutation conferring phenotypes consistent with hyperactive RNAPII mutants which increase RNAPII transcription speed.

To investigate the *in vivo* RNAPII transcription speed of *Arabidopsis* RNAPII carrying the *NRPB2*$_{Y732F}$ mutation, we developed an assay to monitor nascent RNAPII elongation after rapid transcription induction. To avoid time-consuming sample handling and processing issues associated with RNAPII Chromatin Immunoprecipitation from plants (RNAPII-ChIP) [25, 37], we analyzed nascent RNA attached to RNAPII to monitor RNAPII elongation [38]. We identified three pathogen resistance related Toll/interleukin receptor (TIR)–type NB-LRR genes *AT4G19520*, *AT5G41740* and *AT5G41750* genes [39, 40], that are rapidly induced by flagellin 22 treatment. To monitor the "waves" of RNAPII elongation on these three genes after transcriptional induction we performed a time course experiment during flagellin 22 treatment and determined the RNAPII signal by analyzing nascent RNA attached to RNAPII [38]. We chose *NRPB2*$_{WT}$*-FLAG* +/+ Col-0 and *NRPB2*$_{Y732F}$*-FLAG* +/+ Col-0 as material for this assay since we detected no differences growth and immune response in this background. In brief, FLAG-tagged NRPB2$_{WT}$ and NRPB2$_{Y732F}$ proteins were immuno-precipitated by anti-FLAG antibody; RNAPII-associated RNA was purified and used in RT-qPCR analyses of three locations spanning these genes (Fig 2A). When gene induction is well synchronized, fast transcription is expected to show higher nascent RNA level in the gene body and towards the 3' end of candidate genes during flagellin 22 treatment. We found that the candidate genes were rapidly induced by flagellin 22 treatment, as we detected an increase of nascent RNA level at probe 1 of these genes from 0 minutes to 4 minutes after treatment (Fig 2B and C, Figure

EV2E). Furthermore, data for the probe capturing RNAPII transcription shortly after induction (i.e. probe 1) suggests that these genes were induced with similar kinetics and to similar levels in *NRPB2*$_{WT}$ and *NRPB2*$_{Y732F}$. Interestingly, we found that *NRPB2*$_{Y732F}$ showed higher nascent RNA level than *NRPB2*$_{WT}$ at probe 2 and probe 3 located further into the gene, from three minutes of flagellin 22 treatment onwards (Fig 2B and C, Figure EV2E). These data suggest that although wild type and mutant RNAPII were equally induced near the 5' ends of genes, the *NRPB2*$_{Y732F}$ RNAPII reaches the 3' ends of genes earlier than *NRPB2*$_{WT,}$ supporting faster RNAPII transcription of the *NRPB2*$_{Y732F}$ mutants. In summary, we detect evidence that the *Arabidopsis NRPB2*$_{Y732F}$ mutant exhibits accelerated RNAPII transcription *in vivo*.

Accelerated RNAPII transcription reduces promoter-proximal RNAPII stalling

To study the genome-wide effects of accelerated RNAPII transcription speed in *NRPB2*$_{Y732F}$, we performed plant Native Elongating Transcript sequencing (plaNET-seq) to monitor nascent RNAPII transcription [8]. Two independent replicates of plaNET-seq were performed for *NRPB2*$_{Y732F}$ *+/+ nrpb2-2 -/-* mutant and *NRPB2*$_{WT}$ *+/+ nrpb2-2 -/-* control (Fig EV3A and B). Nascent RNA profiling in *Arabidopsis* revealed RNAPII stalling peaks near the beginning of transcription units in promoter-proximal regions. The positioning of the first nucleosome correlates well with the position of promoter-proximal RNAPII stalling in *Arabidopsis* [8]. To address the role of transcription speed in regulating promoter-proximal stalling, we investigated the RNAPII signal in promoter-proximal regions from plaNET-seq in *NRPB2*$_{Y732F}$ *+/+ nrpb2-2 -/- and NRPB2*$_{WT}$ *+/+ nrpb2-2 -/-*. Visual inspection suggested that *NRPB2*$_{Y732F}$ reduced peaks of RNAPII near the 5' ends of genes when compared to *NRPB2*$_{WT}$ (Fig 3A). A metagene plot showing plaNET-seq RNAPII signal in a 1 kb region centered at the +1 nucleosomes [41] revealed that *NRPB2*$_{Y732F}$ reduced promoter-proximal RNAPII stalling centered at the +1 nucleosome position genome-wide compared to *NRPB2*$_{WT}$ (Fig 3B). The metagene-level reduction of RNAPII stalling in *NRPB2*$_{Y732F}$ was confirmed when the plaNET-seq signal was anchored at transcription start sites (TSSs) (Fig EV3C). To further quantify this effect, we calculated the RNAPII stalling index for well-expressed genes (plaNET-seq signal FPKM>10, n=6596), which represents relative enrichment of RNAPII signal at promoter-proximal regions compared to the whole gene body. This analysis quantified a 35% reduction of the median

value of RNAPII promoter-proximal stalling index in *NRPB2*$_{Y732F}$ compared to *NRPB2*$_{WT}$ (Fig 3C). These data illustrate that a restriction of RNAPII transcription speed contributes strongly to the formation of characteristic promoter-proximal RNAPII peaks.

Accelerated transcription increases nascent RNAPII signal in gene bodies

We observed increased RNAPII signals in *NRPB2*$_{Y732F}$ compared to *NRPB2*$_{WT}$ at intragenic positions downstream of promoter proximal stalling sites (Fig EV3D). A metagene analysis of RNAPII activity across gene bodies confirmed this observation on a genome-wide scale (Fig 3D). Increased RNAPII signal in gene bodies could be reconciled by less RNAPII at promoter-proximal stalling regions in *NRPB2*$_{Y732F}$ compared to *NRPB2*$_{WT}$. Consistently, increased nascent transcription in gene bodies in *NRPB2*$_{Y732F}$ correlated with increased plaNET-seq metagene profiles of exons and introns (Fig 3E and F). Interestingly, we detected an accumulation of exonic plaNET-seq signal towards the 3' end of exons in *NRPB2*$_{Y732F}$ (Fig 3E). This effect was insensitive to the exon length (Fig EV3E-G). Exon-intron boundaries may thus trigger a pile-up of nascent RNAPII transcription when transcription is accelerated. In introns, accelerated RNAPII transcription amplifies nascent RNAPII signal compared to *NRPB2*$_{WT}$ and resulted in a uniform accumulation profile, which can be observed in metagene plots for introns of variable length genome-wide (Fig 3F, Fig EV3H-J). We next tested possible connections between increased intragenic nascent RNAPII signal and splicing regulation. However, the fast mutant showed increased signal over both constitutive and alternative exons and introns (Fig EV3K-N). In conclusion, accelerated RNAPII transcription in *NRPB2*$_{Y732F}$ resulted in increased nascent RNAPII transcription in gene bodies.

Accelerated transcription enhances intron splicing and exon skipping

plaNET-seq co-purifies splicing intermediates due to co-transcriptional spliceosome association with RNAPII (Fig 4A). The splicing intermediates appear as single-nucleotide sharp peaks at 5' splicing site (5'SS) and 3' splicing site (3'SS) and thus can be distinguished from the nascent reads [10, 42]. We detected an increased fraction of splicing intermediate reads corresponding to 5'SS in plaNET-seq of *NRPB2*$_{Y732F}$ compared to *NRPB2*$_{WT}$, while no obvious difference could be detected for 3' splicing intermediates (Fig 4B). These data suggested an increased association of accelerated RNAPII transcription with splicing intermediates overlapping a 5'SS. Since 5' splicing intermediates are associated with the spliceosome, we

predicted that higher RNAPII coverage in gene bodies could increase spliceosome association and perhaps enhance splicing in *NRPB2*$_{Y732F}$. To test this idea, two independent replicates of RNA-seq were performed for *NRPB2*$_{Y732F}$ *+/+ nrpb2-2 -/-* and *NRPB2*$_{WT}$ *+/+ nrpb2-2 -/-* seedlings (Fig EV4A). RNA-seq detects predominantly spliced transcripts with a characteristic signal intensity profile matching annotated exons. However, we noticed RNA-seq signal corresponding to some introns, presumably representing regulatory or poorly spliced introns (i.e. retained introns). Interestingly, initial visual inspection of several retained introns indicated that accelerated RNAPII transcription in *NRPB2*$_{Y732F}$ appeared to decrease intronic RNA-seq signal (Fig 4C). Strikingly, this finding is supported by a genome-wide decrease in the fraction of intronic RNA-seq signal across all genes (Fig 4D), suggesting a genome-wide trend of increased splicing efficiency in plants when RNAPII transcription is accelerated. A systematic genome-wide analysis identified 1517 differentially expressed (DE) introns from the RNA-seq data of *NRPB2*$_{Y732F}$ compared to *NRPB2*$_{WT}$. The majority (1334 out of 1517) of DE introns exhibit decreased fraction of intronic reads (Table S2). We identified a similar number of DE exons with increased or decreased expression in *NRPB2*$_{Y732F}$ compare to *NRPB2*$_{WT}$, while we detected many more introns with decreased expression (Fig 4E). Quantification of DE exons revealed a small yet significant reduction of expression (Fig 4F) that we visualized for internal exons of the *AT1G58060* and *AT3G05680* genes (Fig 4G). In contrast, we detected a stronger decrease for DE introns in *NRPB2*$_{Y732F}$ mutant compared to *NRPB2*$_{WT}$ (Fig 4H). We next tested for alternative 5'SS and 3'SS usage (Fig EV4B) in the *NRPB2*$_{Y732F}$ mutant compared to *NRPB2*$_{WT}$ and found a trend to shift 5'SS upstream and 3'SS downstream (Fig EV4C-E). We note that a downstream shift of 3'SS is consistent with effects observed in the splicing factor mutant *ntr1* linked to increased transcription speed in *Arabidopsis [16]*. In summary, our RNA-seq data revealed multiple effects of accelerated RNAPII transcription on splicing in *Arabidopsis*. Our analyses highlighted reduced intron retention as the most notable effect of altered RNAPII activity in *Arabidopsis* on splicing. The data support the idea that inefficient splicing of these introns in wild type may be interpreted through a model where RNAPII transcription speed could be limiting their splicing.

Accelerated RNAPII transcription reduces RNAPII stalling at gene ends

plaNET-seq resolves peaks of RNAPII activity at 3' ends of plant genes. This localized reduction of transcription speed at gene ends may assist RNAPII transcriptional termination. To test this hypothesis, we investigated the RNAPII stalling peaks at 3' ends of genes by plaNET-seq in the fast transcription mutant *NRPB2*$_{Y732F}$ compared to *NRPB2*$_{WT}$. We detected RNAPII stalling downstream of poly (A) sites (PASs) of *Arabidopsis* genes in *NRPB2*$_{WT}$ (Fig 5A). In contrast, PAS-stalling peaks of RNAPII in this region were often undetectable in *NRPB2*$_{Y732F}$, as shown for the *AT2G21410* gene (Fig 5A). A metagene analysis confirmed RNAPII peaks downstream of PAS at 3' gene ends in *NRPB2*$_{WT}$ and a strong reduction in *NRPB2*$_{Y732F}$ genome-wide (Fig 5B). These data connect increased RNAPII transcription speed and reduced RNAPII stalling at gene ends downstream of PAS. If RNAPII stalling were promoting transcription termination, we would expect termination defects in *NRPB2*$_{Y732F}$. Indeed, genome browser screenshots indicated higher RNAPII signal downstream of the PAS-stalling region in *NRPB2*$_{Y732F}$ in comparison with *NRPB2*$_{WT}$ (Fig 5A), suggesting transcriptional read-through as a consequence of increased transcription speed. To quantify this effect genome-wide, we determined the transcriptional read-through lengths in *NRPB2*$_{WT}$ and *NRPB2*$_{Y732F}$. We used a statistical model which was based on empirical distributions of plaNET-seq tag counts in both genic and intergenic regions (see Methods). Strikingly, we observed that *NRPB2*$_{Y732F}$ extended transcriptional read-through genome-wide (FPKM > 5, n=9316) (Fig 5C). We detected a 115 nt increase of median transcriptional read-through length in *NRPB2*$_{Y732F}$ compared to *NRPB2*$_{WT}$ (*NRPB2*$_{Y732F}$, 649 nt; *NRPB2*$_{WT}$, 534 nt) (Fig 5D). *NRPB2*$_{Y732F}$ accelerating transcription speed thus reduces RNAPII termination efficiency and extends transcriptional read-through. The process of RNAPII termination is sensitive to the RNAPII active site and putative catalysis, consistent with a model where increased RNAPII speed alters kinetic competition between transcriptional stalling, termination and further elongation.

Transcriptional read-through blurs the boundaries of transcription units, which could result in overlapping transcripts and potential gene expression conflicts. To investigate this, we focused on read-through transcription of tandemly oriented genes, where transcription read-through from upstream-located genes may invade downstream genes. RNAPII with

accelerated transcription speed is expected to extend transcriptional read-through into the intergenic space (i.e. gaps) between the PAS of an upstream gene and the TSS of a downstream gene (PAS-TSS gaps). Indeed, $NRPB2_{Y732F}$ shows higher RNAPII signal than $NRPB2_{WT}$ in the second half of PAS-TSS gaps (n=5753) while RNAPII in $NRPB2_{WT}$ stalls downstream of PAS in the first half of PAS-TSS gaps (Fig 5E and Fig EV5A). We further investigated plaNET-seq RNAPII signal in PAS-PAS gaps of paired genes facing each other in "tail-to-tail" orientation (n=1384). Also for this subset of genes, $NRPB2_{Y732F}$ lacked the characteristic RNAPII PAS-stalling in the first half of PAS-PAS gaps and showed significantly higher RNAPII signal in the second half of PAS-PAS gaps (Fig 5F and Fig EV5B). These data suggest that accelerated transcription speed triggers transcriptional read-through genome-wide, resulting in overlapping transcripts and potential gene expression conflicts. In conclusion, our data highlight connections between reduced speed of RNAPII transcription at gene ends (i.e. PAS-stalling) and the termination of RNAPII transcription, linking the speed of transcription to spatial separation of plant transcription units.

Our findings highlight molecular and organismal consequences of altered RNAPII elongation speed in a multi-cellular organism. The two main peaks of RNAPII localization in genomes at gene boundaries were depleted when transcription speed was accelerated (Fig 6A and B). Accelerated RNAPII transcription impacted gene expression after transcriptional initiation, through profound effects on splicing and transcriptional termination. Our data support that transcription speed control at gene boundaries is a key step in gene expression of multicellular organisms.

Discussion

RNAPII transcription speed and organismal development

While we succeeded in generation of viable plants carrying a fast RNAPII mutation, we were unable to obtain plants with a mutation in a conserved residue that reduced RNAPII transcription speed in yeast. This observation is reminiscent of embryonic lethality in mice through a point mutation in the largest RNAPII subunit that decreases transcription speed [43]. Female germline development in *Arabidopsis* involves more complex cellular differentiation than male germline development [44]. A genetic dissection of factors required for female

germline development revealed cell specification by multiple splicing factors [44, 45]. Accelerated RNAPII transcription in *NRPB2*$_{Y732F}$ was associated with increased splicing efficiency, perhaps offering an explanation for enhanced viability of the female gametophyte compared to *nrpb2-2*.

Accelerated RNAPII transcription and RNAPII stalling

Promoter-proximal stalling represents a common feature of transcription throughout eukaryotic genomes [46]. The purpose of promoter-proximal RNAPII stalling is debated actively, yet a reduction of RNAPII transcription speed during stalling could be part of a checkpoint regulating gene expression. In organisms without NELF, for example plants, promoter-proximal RNAPII stalling correlates with the position of first nucleosome encountered by the transcription machinery[8]. Accelerated transcription in *NRPB2*$_{Y732F}$ decreased promoter-proximal stalling and resulted in increased intragenic RNAPII transcription. Our data thus suggest that a reduction of RNAPII elongation speed near promoters facilitates the accumulation of promoter-proximal RNAPII peaks. In *Arabidopsis*, these peaks form independently of NELF, and perhaps form through contributions by nucleosome barriers that correlate well with the peak position [8, 47].

Possible advantages of promoter-proximal RNAPII stalling include a reduced response time to adjust gene expression to new environmental conditions. Instead of initiating the process of RNAPII transcription from recruitment and complex assembly, stalled RNAPII may represent pre-assembled and elongation competent RNAPII complexes waiting for signals to transcribe the full gene [1]. Defense signaling is crucial for plant fitness and regulated with fast temporal dynamics, perhaps achieved by a release of RNAPII into elongation from promoter-proximal stalling sites. If true, this would predict constitutive defense signaling when transcription is accelerated. Interestingly, *NRPB2*$_{Y732F}$ *+/+ nrpb2-2 -/-* plants resembled mutants with constitutively active defense signaling [34]. PR gene induction represents a diagnostic molecular hallmark of elevated defense signaling [48]. While alternative molecular explanations for stunted growth in *NRPB2*$_{Y732F}$ *+/+ nrpb2-2 -/-* may exist, for example indirect effects, the induction of PR gene expression is consistent with an auto-immunity phenotype triggered by accelerated transcription. Our data thus provide a potential connection between plant defense signaling, promoter-proximal RNAPII stalling and the speed of RNAPII

transcription. In conclusion, these data imply that transcription speed limits at gene boundaries may benefit plants by avoiding constitutive defense signaling that triggers auto-immunity.

Accelerated RNAPII transcription and RNA Processing

Our targeted introduction of candidate point mutations represents a direct approach to address mechanistic links between the speed of RNAPII transcription and RNA processing. Nevertheless, some molecular effects we reported could represent indirect effects caused by differences in growth and development between *NRPB2*$_{Y732F}$ *+/+ nrpb2-2 -/-* and *NRPB2*$_{WT}$ *+/+ nrpb2-2 -/-*. RNA-seq revealed that intron retention is reduced when RNAPII is accelerated, in other words, splicing efficiency of poorly spliced introns is increased. plaNET-seq data indicate that increased splicing efficiency is associated with the capture of splicing intermediates with 3' terminal bases overlapping 5'SS, perhaps indicating that splicing of retained introns could be increased by promoting RNAPII binding to 5'SS. In conclusion, the speed of RNAPII transcription contributes to plant gene expression by modulating splicing efficiency, particularly at retained introns.

plaNET-seq data informed on transcriptional termination of RNAPII. Strikingly, we found a reduction of RNAPII peaks associated with termination when transcription is accelerated, and an increased distance of read-through transcription downstream of the PAS (Fig 5D). Read-through transcription triggered by elevated temperature has been reported in budding yeast and mammalian cell culture [37, 49]. Extended read-through as observed in an accelerated RNAPII transcription mutant may have functional consequences on gene expression. The increased transcriptional read-through may result in gene expression defects for neighboring genes, for example by transcriptional interference [50, 51]. In summary, our data support the idea that a reduction of RNAPII transcription speed promotes RNAPII density peaks in genomes with functional consequences for the process of transcriptional termination.

CONTACT FOR REAGENT AND RESOURCE SHARING

Please contact S.M. (sebastian.marquardt@plen.ku.dk) for reagents and resources generated in this study.

MATERIALS AND METHODS

REAGENT or RESOURCE	SOURCE	IDENTIFIER
Antibodies		
Rabbit Anti-Mouse Immunoglobulins/HRP	Dako	P0161; RRID:AB_2687969
Swine anti-rabbit Ig HRP antibody	Dako	P0217; RRID:AB_2728719
Anti-Histone H3 antibody	abcam	Ab1791; RRID:AB_302613
Monoclonal ANTI-FLAG® M2 antibody produced in mouse	Sigma-Aldrich	F3165; RRID: AB_259529
Monoclonal ANTI-FLAG® M2 antibody produced in mouse	Sigma-Aldrich	F1804; RRID:AB_262044
Bacterial and Virus Strains		
E. coli DH5α™ Competent Cells	Thermo Fisher	Cat no. 18265017
A. tumefaciens GV3101(PMP90)	N/A	N/A
Peptides		
Flg22 peptides	Schafer-N	Peptide 40007
Critical Commercial Assays		
miRNeasy Mini Kit	QIAGEN	ID: 217004
SuperScript™ IV First-Strand Synthesis System	invitrogen	Cat. no.18091050
NEXTflex Small RNA-Seq Kit v3	Bioo Scientific	N/A
DNA High Sensitivity kit	Agilent	5067-4626
4–15% Criterion™ TGX Stain-Free™ Protein Gel	BIO-RAD	Cat. no. 5678084
TURBO DNA-free kit	Thermo Fisher	Cat. no. AM1907
Dynabeads™ Antibody Coupling Kit	Thermo Fisher	Cat. no. 114311D
TruSeq RNA Library Prep Kit v2	illuminia	RS-122-2001
GoTaq® qPCR Master Mix	Promega	Cat no. A6002
RNeasy Plant Mini Kit	QIAGEN	ID: 74904
Deposited Data		
GSE133143	NCBI GEO	token: ibqrewsijvuhfgr
Experimental Models: Organisms/Strains		
Arabidopsis thaliana Col-0	N/A	N/A
NRPB2/nrpb2-2 mutant	Dr. Craig Pikaard	N/A
Software and Algorithms		
Software for bioinformatic analysis: See Methods	GitHub	https://github.com/Maxim-Ivanov/Leng_et_al_2019

REAGENTS AND TOOLS TABLE

METHODS AND PROTOCOLS

Plant material and growth conditions

The *Arabidopsis* mutant lines generated in this study were based on *Arabidopsis thaliana* Columbia ecotype (Col-0) background. Generation of transgenic *Arabidopsis* plants was performed by *Agrobacterium*-mediated transformation as described [52]. *NRPB2*$_{Y732F}$ and *NRPB2*$_{WT}$ transgenes were first introduced to Col-0 then crossed with *nrpb2-2* +/- mutant. *NRPB2*$_{WT}$ *+/+ nrpb2-2 -/-* and *NRPB2*$_{Y732F}$ *+/+ nrpb2-2 -/-* double mutants were screened by genotyping from F3 generation (Fig EV1A).

For *in vitro* growth, *Arabidopsis* seeds were surface sterilized and placed on ½ MS media agar plates (1% sucrose). The seeds were stratified in 4°C for 3 days before transferred into 22°C with 16/8 h light/dark. For flagellin 22 treatment experiments, *Arabidopsis* seeds were on ½ MS media agar plate (1% sucrose) for 12 days, seedlings were transferred into ½ MS liquid media (1% sucrose) and grew in flasks under 22°C with 16/8 h light/dark and 150 rpm shaking for 2 days. For growth on soil, *Arabidopsis* seeds were sowed on soil directly and undergo stratification in 4°C for 3 days before growth under 22°C with 16/8 h light/dark on soil.

Plasmid Construction

The construction of vectors *Agrobacterium*-mediated stable transformation was based on pEarleyGate 302 vector (pEG302). pEG302-AtNRPB2$_{WT}$-FLAG construct was kindly provided by Craig Pikaard [33]. To generate pEG302-AtNRPB2$_{Y732F}$-FLAG and pEG302-AtNRPB2$_{Y732F}$-FLAG, pEG302-AtNRPB2$_{WT}$-FLAG construct was linearized by DraIII digestion and used as backbone in isothermal assembly reactions; the inserts in isothermal assembly are partial genomic NRPB2 sequences containing Y732F (TAT to TTT) point mutation and P979S (CCG to TCG), respectively. Fragment containing DNA mutation for Y732F mutant was generated by overlapping PCR (primer pair 3089/3082) fusing two fragments generated by primer pair 3089/3467 and 3082/3466. By using similar strategy, fragment containing DNA mutation for P979S mutant was also generated by overlapping PCR (primer pair 3089/3082) fusing two fragments generated by primer pair 3089/3084 and 3082/3083. Isothermal assembly was performed subsequently to generate pEG302-AtNRPB2$_{Y732F}$-FLAG and pEG302-

AtNRPB2$_{Y732F}$-FLAG. All constructs were verified by extensive restriction enzyme digestions and the fragment with DNA mutations for *NRPB2*$_{Y732F}$ and *NRPB2*$_{WT}$ were confirmed by DNA sequencing analysis. The primers used in plasmid construction are listed in Table S1.

Flagellin treatment

Flagellin 22 (N-terminus acetylated) was synthesized by Schafer-N (schafer-n.com). For each replicate, flagellin 22 treatment was carried out by adding the 0.75 ml flagellin 22 solution (1 mg/ml in DMSO) to *Arabidopsis* seedlings from 50 µL seeds growing in 100 mL liquid MS media in a flask (3.3 µM as final concentration of flagellin 22). The treatment was set in 0 minutes (before treatment), 2 minutes, 3 minutes and 4 minutes time course. Each experiment was performed in 3 independent replicates. After flagellin 22 treatment, the seedlings were flash-frozen in liquid nitrogen.

Protein extraction and western blotting

NRPB2$_{WT}$-FLAG, NRPB2$_{Y732F}$-FLAG and NRPB2$_{P979S}$-FLAG proteins were extracted from 2-week-old *Arabidopsis* seedlings of *NRPB2*$_{WT}$ +/+ Col-0, *NRPB2*$_{Y732F}$ +/+ Col-0 and *NRPB2*$_{P979S}$ +/+ Col-0, respectively. Equal amounts of plant material were ground into a fine powder and proteins were extracted in 2.5x extraction buffer (150 mM Tris-HCl pH 6.8; 5% SDS; 25% Glycerol; 0.025% Bromophenol blue; 0.1 mM DTT). Total proteins were separated by SDS-PAGE on precast 4–15% Criterion TGX stain-free protein gels (Bio-Rad) and transferred to PVDF membrane by Trans-blot Turbo transfer system (Bio-Rad). 5% non-fat milk in PBS was used to block blotted membrane (30 minutes at room temperature). Anti-FLAG (Sigma F1804 or F3165) antibodies and anti-mouse HRP-conjugated secondary antibody (Dako P0161) were used as primary and secondary antibodies for the detection of FLAG-tagged NRPB2 proteins. Anti-H3 (abcam ab1791) antibody and anti-rabbit HRP-conjugated secondary antibody (Dako P0217) were used as primary and secondary antibodies for the detection of histone H3. The membrane was incubated with primary antibody overnight at 4°C with gentle rotation (final concentration 0.25 µg/mL in PBS). Membranes were washed with PBS and then incubated with secondary antibody (1:10000 dilution in PBS) for 1 hour at room temperature, followed by 2 times washes with PBS (5 minutes each) and 1 time wash with PBST (10 minutes). Chemiluminescent signals were detected using Super-Signal West Pico Chemiluminescent (Thermo Fisher Scientific) according to manufacturer's instructions.

444 **Yeast strains, media and primer extension analysis**

445 Yeast media are prepared as described [27]. For MPA and Mn^{2+} growth assay, MPA (final
446 concentration 20 mg/ml) and $MnCl_2$ (15 mM) was supplemented to minimal SC-Leucine
447 medium. The yeast RNAPII mutant strains were generated by site-directed mutagenesis as
448 previously described [20]. Transcription start site selection of *ADH1* gene was assayed by
449 primer extension analysis. In brief, corresponding yeast strains were grown in YPD media to
450 mid-log phase; 30 µg of isolated yeast total RNA from each indicated strains were used in
451 primer extension analysis exactly as previously described [20, 27].

452 **Nascent RNA isolation**

453 Nascent RNA was isolated according to previously described protocol with minor changes [38].
454 $NRPB2_{WT}$ +/+ Col-0, $NRPB2_{Y732F}$ +/+ Col-0 seedlings from flagellin 22 treatment were ground
455 into a fine powder. Nuclei were isolated and washed with HONDA buffer (0.44 M sucrose, 1.25%
456 Ficoll, 2.5% Dextran T40, 20 mM Tris-HCl pH 7.5, 10 mM $MgCl_2$, 0.5% Triton X-100, 5 mM
457 DTT, 1× EDTA-free Complete protease inhibitor (Roche)). The nuclear fraction was digested
458 by 600 U DNase I in 0.5 mL Lysis buffer (0.3 M NaCl, 20 mM Tris-HCl pH 7.5, 5 mM MgCl2, 5
459 mM β-mercaptoenthanol, 1× EDTA-free Complete protease inhibitor (Roche), 0.5% Tween-20,
460 10 µL RNase inhibitor (moloX GmbH, www.molox.de)) at 4°C for 20 minutes with shaking at
461 2000 rpm. The supernatant of a centrifugation (10000 g for 10 minutes at 4°C) was recovered
462 into a new tube and combined with Dynabeads M-270 (Invitrogen) coupled with anti-FLAG
463 antibody (Sigma) for 2 hours at 4°C with gentle rotation. Anti-FLAG antibody was coupled with
464 Dynabeads according to the manufacturer's instructions. After FLAG-IP, beads were washed 6
465 times using 0.5 mL Wash buffer (0.3 M NaCl, 20 mM Tris-HCl pH 7.5, 5 mM $MgCl_2$, 5 mM β-
466 mercaptoenthanol, 1× EDTA-free Complete protease inhibitor (Roche) and RNase inhibitor).
467 Bead-bound protein was eluted with 0.5 mg/ml 3xFLAG peptide (ApexBio) for 30 minutes twice
468 at 4°C. RNA attached to immunoprecipitated proteins was isolated using QIAGEN miRNeasy
469 Mini Kit according to manufacturer's instructions. Western blot has been done as previously
470 described [38] for input, unbound and eluted fractions to monitor IP efficiency.

471 **Nascent RNA analysis**

472 Isolated nascent RNA was treated with Turbo DNase to remove DNA contamination following
473 the manufactural instruction (Ambion). Hundred nanograms of DNase-treated RNA was used

for reverse transcription into cDNA by gene specific primers following the manufactural instruction of Superscript IV (Invitrogen) kit. Quantitative analysis of the generated cDNA was carried out by qPCR using the GoTaq qPCR Master Mix (Promega) and CFX384 Touch Real-Time PCR Detection System (Biorad). Negative controls lacking the reverse transcriptase enzyme (-RT) were performed alongside all RT–qPCR experiments. qPCR expression level of each primer pair was calculated relative to the level of reference gene *ACT2.* All the primers used in RT and qPCR were summarized in Table S1.

PlaNET-seq library construction and sequencing

Libraries for plaNET-seq were prepared as previously described [8]. Nascent RNA from *NRPB2$_{WT}$ +/+ nrpb2-2 -/-* and *NRPB2$_{Y732F}$ +/+ nrpb2-2 -/-* seedlings was used in plaNET-seq. In specific, the plaNET-seq libraries were constructed according to Bioo Scientific's NEXTflex Small RNA-Seq kit v3 using a customized protocol. Two independent replicate libraries were constructed for each plant genotype. Approximately 100 ng RNA was used for each replicate. The isolated RNA was ligated with 3'-linker and fragmented in alkaline solution (100 mM $NaCO_3$ pH 9.2, 2 mM EDTA). The fragmented RNA was cleaned up and subjected to T4 PNK treatment (20 U PNK, NEB) for 20 minutes at 37°C followed by re-annealing of RT primer (5'-GCCTTGGCACCCGAGAATTCCA-3'; 70^{0}C, 5 minutes; 37^{0}C, 30 minutes; 25^{0}C, 15 minutes). The RNA was then re-introduced to the manufacturer's protocol at the adapter inactivation step. The final libraries were quantified with DNA High Sensitivity kit on Agilent Bioanalyzer 2100 and then sequenced on the Illumina HiSeq 4000 platform in PE150 mode at Novogene (en.novogene.com).

Total RNA extraction and RNA-seq

Total RNA was extracted from 2-week-old *NRPB2$_{WT}$ +/+ nrpb2-2 -/-* and *NRPB2$_{Y732F}$ +/+ nrpb2-2 -/- Arabidopsis* seedlings using Plant RNeasy Mini Kit following manufactural instructions (QIAGEN). Turbo DNase (Ambion) was used to treat extracted RNA using oligo-dT primers and Superscript IV (Invitrogen) as per manufacturer's instructions. The poly(A)-enriched libraries for RNA-seq were constructed using Illumina TruSeq Sample Prep Kit v2 following the manufacturer's protocol and quantified on Agilent 2100 Bioanalyzer. The sequencing was performed on Illumina HiSeq 4000 platform in PE100 mode.

Bioinformatics

All the supporting code for bioinformatics analysis is available at https://github.com/Maxim-Ivanov/Leng_et_al_2019.

Alignment and post-processing of plaNET-seq reads was done as previously described [8]. The first 4 bases of both R1 and R2 reads in plaNET-Seq are Unique Molecular Identifiers (UMIs). They were trimmed from read sequences and appended to read names using UMI-Tools v0.5.3. After UMI trimming, the 5'-terminal base of R2 corresponds to the 3'-end of original RNA molecule and thus denoted the genomic position of RNAPII active center. R2 reads were aligned to TAIR10 genome assembly using STAR v2.5.2b in transcriptome-guided mode with the following settings: --outSAMmultNmax 1 --alignEndsType Extend5pOfRead1 --clip3pAdapterSeq GATCGTCGGACT. Ensembl Plants release 28 was used as the source of transcript annotation for alignment. The BAM files were sorted using Samtools v1.3.1. The following categories of reads were filtered out: i) PCR duplicates (UMI-Tools); ii) Reads aligned within 100 bp from any rRNA, tRNA, snRNA or snoRNA gene from Araport11 on either strand (BEDtools v2.17.0); iii) Reads aligned with MAPQ < 10 (Samtools). The filtered BAM files were imported into R environment v3.5.1 using GenomicAlignments_1.18.1 library. The strand orientation of reads was flipped to restore strandness of the original RNA molecules. 3'-terminal bases of flipped reads were found to overlap with donor or acceptor splice sites much more frequently than could be expected by chance. Such reads most likely represent splicing intermediates due to co-immunoprecipitation of the spliceosome together with FLAG-tagged RNAPII complexes. These reads were filtered out by overlap with the union of splice sites obtained from both Ensembl Plants 28 (TxDb.Athaliana.BioMart.plantsmart28 package) and Araport11 annotations. In addition, all split reads were removed as possible mature RNA contaminations. The remaining reads are expected to represent the nascent RNA population. Their genomic coverage was exported as strand-specific BigWig and bedgraph files using rtracklayer_1.42.2. For details on the alignment procedure, see 01-Alignment_of_plaNET-Seq_data.sh and 02-Postprocessing_of_plaNET-Seq_data.R.

Araport11 annotation was used throughout all further steps of data analysis because it is more comprehensive in terms of non-coding transcripts than both TAIR10 and Ensembl Plants 28 annotations. We adjusted gene borders from Araport11 using coordinates of TSS and PAS tag

clusters which were called using CAGEfightR package [53] from the available TSS-seq [50] and Direct RNA-seq datasets [54, 55], respectively. If multiple TSS or PAS tag clusters were connected to the same gene, the strongest of them was chosen as the new border. For details, see 03_Adjustment_of_Araport11_gene_boundaries.

To draw metagene plots of plaNET-seq, we merged Bedgraph tracks of the two biological replicates of each genotype. The merged tracks were then normalized to 1 million reads in nuclear protein-coding genes. The X axes of metagene plots represent the genomic intervals of choice (whole genes, exons, introns etc) which were scaled to the defined number of bins. Intervals overlapping multiple annotated transcription units were excluded from consideration. Both introns and exons were trimmed by 5 bp each side prior to scaling to avoid possible artifacts. The Y axes show the sequencing coverage averaged between the genomic intervals. The shaded area in metagene plots represents normal-based standard error of mean of normalized plaNET-seq signal at each genomic bin. For details, see 08-Metagene_plots.R. The positions of nucleosomes in Arabidopsis were obtained from the PlantDHS database [56].

To calculate the read-through (RT) length, we considered transcribed genes (plaNET-seq FPKM in WT samples above 5). Genomic intervals for RT length estimation were defined from PAS of the analyzed gene to the nearest downstream TSS. Coordinates of TSS and PAS clusters were called from TSS-seq and Direct RNA-seq datasets as described above. For each gene of interest, the empirical distribution of plaNET-seq tag counts in 100 bp sliding window was obtained (the "transcription" model). The "random" model corresponding to the un-transcribed state was represented by Poisson distribution where the rate parameter was estimated from plaNET-seq tag counts in intergenic regions. Then plaNET-seq tags were counted in every 100 bp window moving in 10 bp steps along the candidate RT genomic interval. For each window, the probability to observe at most this tag count under the gene-specific "transcription" model was divided by the probability to observe at least this tag count under the alternative "random" model. The start position of the first window where the probability ratio dropped below 1 was considered as the end of the read-through region. For details, see 04-Read-through_distance.R.

To calculate promoter-proximal RNAPII stalling index for each gene, we first found 100 bp windows with the highest plaNET-seq coverage within the interval (TSS - 100 bp, TSS + 300

bp). Center of this window was considered as the summit of promoter-proximal RNAPII peak. The stalling index was then calculated as the ratio of plaNET-Seq coverage in this window vs the whole gene (normalized by gene width). To avoid statistical artifacts, genes shorted than 1 Kb or having plaNET-seq FPKM below 1 were skipped from consideration. For details, see 05-Promoter-proximal_stalling_index.R.

RNA-Seq reads were adapter- and quality trimmed by TrimGalore v0.4.3 in paired-end mode and then aligned to TAIR10 by STAR v2.5.2b in local mode. Aligned reads with MAPQ below 10 were removed by Samtools v1.3.1. BAM files were converted to un-stranded Bedgraph and BigWig files using BEDtools genomecov v2.26.0 and kentUtils bedGraphToBigWig v4, respectively. The code was detailed in the section 06-Alignment_of_RNA-Seq_data.sh in the mentioned GitHub page.

Differentially expressed genes were called from RNA-Seq data using DESeq2 [57]. Differential expressed exons and introns were detected independently from the changes in gene expression level by DEXSeq [58]. Exons and introns were defined as disjoint exonic or intronic intervals, respectively, in Araport11. For details, see 07-Differential_expression.R.

To detect the differential usage of alternative 5' and 3' splice sites, transcript isoforms were first quantified by Cufflinks [59]. Then the Cufflinks output was used to quantify the different alternative splicing events extracted from an *Arabidopsis* reference transcript dataset AtRTD2 [60] with SUPPA2 [61]. For details, see 10-SUPPA2_pipeline.sh and 11-Differential_AS.R scripts.

Data availability

The raw and processed plaNET-seq and RNA-seq data were deposited in Gene Expression Omnibus (https://www.ncbi.nlm.nih.gov/geo/) under accession number GSE133143 (reviewer token: ibqrewsijvuhfgr).

Acknowledgements:

Research in the laboratory of S.M. is supported by a Hallas-Møller Investigator award by the Novo Nordisk Foundation NNF15OC0014202 and a Copenhagen Plant Science Centre Young Investigator Starting grant. In addition, this project has received funding from the European Research Council (ERC) and the Marie Curie Actions under the European Union's Horizon 2020 research and innovation programme StG2017-757411 (S.M.) and MSCA-IF 703085 (P.K.). Research in the laboratory of C.D.K. is supported by NIH R01GM097260. We are grateful to Mary Gehring and Steve Buratowski for support during early stages of this project, and Morgan Moeglein for excellent plant care. We are grateful to Craig Pikaard for sharing key reagents. We thank the members of the Marquardt lab for feedback on the manuscript.

Author Contributions

Conceptualization, X.L., C.K. and S.M.; Methodology, M.I., P.K. and S.M.; Investigation, X.L., P.K., I.M., M.I. and S.M.; Formal Analysis, M.I., A.T. and A.S; Data Curation, M.I.; Writing-Original Draft, X.L. and S.M; Writing-Review & Editing, X.L., M.I., C.K., P.K., P.B., A.S. and S.M.; Visualization, X.L. and M.I.; Resources, C.K. and S.M.; Supervision, C.K. and S.M.; Funding Acquisition, S.M.

Declaration of Interests

The authors declare no competing interests.

References

1. Jonkers I, Lis JT (2015) Getting up to speed with transcription elongation by RNA polymerase II. *Nature reviews Molecular cell biology* **16**: 167-77
2. Gromak N, West S, Proudfoot NJ (2006) Pause sites promote transcriptional termination of mammalian RNA polymerase II. *Molecular and cellular biology* **26**: 3986-96

3. Proudfoot NJ (2016) Transcriptional termination in mammals: Stopping the RNA polymerase II juggernaut. *Science* **352**: aad9926
4. Mahat DB, Salamanca HH, Duarte FM, Danko CG, Lis JT (2016) Mammalian Heat Shock Response and Mechanisms Underlying Its Genome-wide Transcriptional Regulation. *Molecular cell* **62**: 63-78
5. Steurer B, Janssens RC, Geverts B, Geijer ME, Wienholz F, Theil AF, Chang J, Dealy S, Pothof J, van Cappellen WA*, et al.* (2018) Live-cell analysis of endogenous GFP-RPB1 uncovers rapid turnover of initiating and promoter-paused RNA Polymerase II. *Proceedings of the National Academy of Sciences of the United States of America* **115**: E4368-E4376
6. Krebs AR, Imanci D, Hoerner L, Gaidatzis D, Burger L, Schubeler D (2017) Genome-wide Single-Molecule Footprinting Reveals High RNA Polymerase II Turnover at Paused Promoters. *Molecular cell* **67**: 411
7. Vos SM, Farnung L, Urlaub H, Cramer P (2018) Structure of paused transcription complex Pol II-DSIF-NELF. *Nature* **560**: 601
8. Kindgren P, Ivanov M, Marquardt S (2019) Native elongation transcript sequencing reveals temperature dependent dynamics of nascent RNAPII transcription in Arabidopsis. *Nucleic Acids Res* gkz1189. doi: 10.1093/nar/gkz1189
9. Mayer A, di Iulio J, Maleri S, Eser U, Vierstra J, Reynolds A, Sandstrom R, Stamatoyannopoulos JA, Churchman LS (2015) Native elongating transcript sequencing reveals human transcriptional activity at nucleotide resolution. *Cell* **161**: 541-554
10. Nojima T, Gomes T, Grosso ARF, Kimura H, Dye MJ, Dhir S, Carmo-Fonseca M, Proudfoot NJ (2015) Mammalian NET-Seq Reveals Genome-wide Nascent Transcription Coupled to RNA Processing. *Cell* **161**: 526-540
11. Fong N, Kim H, Zhou Y, Ji X, Qiu JS, Saldi T, Diener K, Jones K, Fu XD, Bentley DL (2014) Pre-mRNA splicing is facilitated by an optimal RNA polymerase II elongation rate. *Gene Dev* **28**: 2663-2676
12. Laitem C, Zaborowska J, Isa NF, Kufs J, Dienstbier M, Murphy S (2015) CDK9 inhibitors define elongation checkpoints at both ends of RNA polymerase II-transcribed genes. *Nat Struct Mol Biol* **22**: 396-U71

13. Cramer P, Bushnell DA, Kornberg RD (2001) Structural basis of transcription: RNA polymerase II at 2.8 angstrom resolution. *Science* **292**: 1863-76
14. Vassylyev DG, Vassylyeva MN, Zhang JW, Palangat M, Artsimovitch I, Landick R (2007) Structural basis for substrate loading in bacterial RNA polymerase. *Nature* **448**: 163-U4
15. Wang D, Bushnell DA, Westover KD, Kaplan CD, Kornberg RD (2006) Structural basis of transcription: role of the trigger loop in substrate specificity and catalysis. *Cell* **127**: 941-54
16. Dolata J, Guo YW, Kolowerzo A, Smolinski D, Brzyzek G, Jarmolowski A, Swiezewski S (2015) NTR1 is required for transcription elongation checkpoints at alternative exons in Arabidopsis. *Embo J* **34**: 544-558
17. Herz MAG, Kubaczka MG, Brzyzek G, Servi L, Krzyszton M, Simpson C, Brown J, Swiezewski S, Petrillo E, Kornblihtt AR (2019) Light Regulates Plant Alternative Splicing through the Control of Transcriptional Elongation. *Molecular cell* **73**: 1066
18. Sheridan RM, Fong N, D'Alessandro A, Bentley DL (2019) Widespread Backtracking by RNA Pol II Is a Major Effector of Gene Activation, 5' Pause Release, Termination, and Transcription Elongation Rate. *Molecular cell* **73**: 107-118 e4
19. Cheung AC, Cramer P (2011) Structural basis of RNA polymerase II backtracking, arrest and reactivation. *Nature* **471**: 249-53
20. Qiu CX, Erinne OC, Dave JM, Cui P, Jin HY, Muthukrishnan N, Tang LK, Babu SG, Lam KC, Vandeventer PJ*, et al.* (2016) High-Resolution Phenotypic Landscape of the RNA Polymerase II Trigger Loop. *Plos Genet* **12**: e1006321
21. Malik I, Qiu CX, Snavely T, Kaplan CD (2017) Wide-ranging and unexpected consequences of altered Pol II catalytic activity in vivo. *Nucleic Acids Res* **45**: 4431-4451
22. Kireeva ML, Nedialkov YA, Cremona GH, Purtov YA, Lubkowska L, Malagon F, Burton ZF, Strathern JN, Kashlev M (2008) Transient reversal of RNA polymerase II active site closing controls fidelity of transcription elongation. *Molecular cell* **30**: 557-66
23. Malagon F, Kireeva ML, Shafer BK, Lubkowska L, Kashlev M, Strathern JN (2006) Mutations in the Saccharomyces cerevisiae RPB1 gene conferring hypersensitivity to 6-azauracil. *Genetics* **172**: 2201-9

24. Kaplan CD, Larsson KM, Kornberg RD (2008) The RNA polymerase II trigger loop functions in substrate selection and is directly targeted by alpha-amanitin. *Molecular cell* **30**: 547-56
25. Mason PB, Struhl K (2005) Distinction and relationship between elongation rate and processivity of RNA polymerase II in vivo. *Molecular cell* **17**: 831-840
26. Powell W, Reines D (1996) Mutations in the second largest subunit of RNA polymerase II cause 6-azauracil sensitivity in yeast and increased transcriptional arrest in vitro. *The Journal of biological chemistry* **271**: 6866-73
27. Kaplan CD, Jin HY, Zhang IL, Belyanin A (2012) Dissection of Pol II Trigger Loop Function and Pol II Activity-Dependent Control of Start Site Selection In Vivo. *Plos Genet* **8**: 172-188
28. Corden JL (2013) RNA polymerase II C-terminal domain: Tethering transcription to transcript and template. *Chemical reviews* **113**: 8423-55
29. Soares LM, He PC, Chun Y, Suh H, Kim T, Buratowski S (2017) Determinants of Histone H3K4 Methylation Patterns. *Molecular cell* **68**: 773-785 e6
30. Fong N, Saldi T, Sheridan RM, Cortazar MA, Bentley DL (2017) RNA Pol II Dynamics Modulate Co-transcriptional Chromatin Modification, CTD Phosphorylation, and Transcriptional Direction. *Molecular cell* **66**: 546-557 e3
31. Wang D, Bushnell DA, Huang XH, Westover KD, Levitt M, Kornberg RD (2009) Structural Basis of Transcription: Backtracked RNA Polymerase II at 3.4 Angstrom Resolution. *Science* **324**: 1203-1206
32. Da LT, Pardo-Avila F, Xu L, Silva DA, Zhang L, Gao X, Wang D, Huang X (2016) Bridge helix bending promotes RNA polymerase II backtracking through a critical and conserved threonine residue. *Nature communications* **7**: 11244
33. Onodera Y, Nakagawa K, Haag JR, Pikaard D, Mikami T, Ream T, Ito Y, Pikaard CS (2008) Sex-biased lethality or transmission of defective transcription machinery in Arabidopsis. *Genetics* **180**: 207-18
34. Petersen M, Brodersen P, Naested H, Andreasson E, Lindhart U, Johansen B, Nielsen HB, Lacy M, Austin MJ, Parker JE*, et al.* (2000) Arabidopsis map kinase 4 negatively regulates systemic acquired resistance. *Cell* **103**: 1111-20

35. Braberg H, Jin H, Moehle EA, Chan YA, Wang S, Shales M, Benschop JJ, Morris JH, Qiu C, Hu F*, et al.* (2013) From structure to systems: high-resolution, quantitative genetic analysis of RNA polymerase II. *Cell* **154**: 775-88
36. Cabart P, Jin H, Li L, Kaplan CD (2014) Activation and reactivation of the RNA polymerase II trigger loop for intrinsic RNA cleavage and catalysis. *Transcription* **5**: e28869
37. Hazelbaker DZ, Marquardt S, Wlotzka W, Buratowski S (2013) Kinetic Competition between RNA Polymerase II and Sen1-Dependent Transcription Termination. *Molecular cell* **49**: 55-66
38. Kindgren P, Ard R, Ivanov M, Marquardt S (2018) Transcriptional read-through of the long non-coding RNA SVALKA governs plant cold acclimation. *Nature communications* **9**: 4561
39. Bomblies K, Lempe J, Epple P, Warthmann N, Lanz C, Dangl JL, Weigel D (2007) Autoimmune response as a mechanism for a Dobzhansky-Muller-type incompatibility syndrome in plants. *Plos Biol* **5**: 1962-1972
40. Sano S, Aoyama M, Nakai K, Shimotani K, Yamasaki K, Sato MH, Tojo D, Suwastika IN, Nomura H, Shiina T (2014) Light-dependent expression of flg22-induced defense genes in Arabidopsis. *Frontiers in plant science* **5**: 531
41. Zhang T, Zhang WL, Jiang JM (2015) Genome-Wide Nucleosome Occupancy and Positioning and Their Impact on Gene Expression and Evolution in Plants. *Plant Physiol* **168**: 1406-U1530
42. Nojima T, Rebelo K, Gomes T, Grosso AR, Proudfoot NJ, Carmo-Fonseca M (2018) RNA Polymerase II Phosphorylated on CTD Serine 5 Interacts with the Spliceosome during Co-transcriptional Splicing. *Molecular cell* **72**: 369-379 e4
43. Maslon MM, Braunschweig U, Aitken S, Mann AR, Kilanowski F, Hunter CJ, Blencowe BJ, Kornblihtt AR, Adams IR, Caceres JF (2019) A slow transcription rate causes embryonic lethality and perturbs kinetic coupling of neuronal genes. *Embo J* **38**: e101244
44. Schmidt A, Schmid MW, Grossniklaus U (2015) Plant germline formation: common concepts and developmental flexibility in sexual and asexual reproduction. *Development* **142**: 229-41

45. Gross-Hardt R, Kagi C, Baumann N, Moore JM, Baskar R, Gagliano WB, Jurgens G, Grossniklaus U (2007) LACHESIS restricts gametic cell fate in the female gametophyte of Arabidopsis. *Plos Biol* **5**: e47
46. Mayer A, Landry HM, Churchman LS (2017) Pause & go: from the discovery of RNA polymerase pausing to its functional implications. *Current opinion in cell biology* **46**: 72-80
47. Ehrensberger AH, Kelly GP, Svejstrup JQ (2013) Mechanistic interpretation of promoter-proximal peaks and RNAPII density maps. *Cell* **154**: 713-5
48. Uknes S, Mauch-Mani B, Moyer M, Potter S, Williams S, Dincher S, Chandler D, Slusarenko A, Ward E, Ryals J (1992) Acquired resistance in Arabidopsis. *The Plant cell* **4**: 645-56
49. Vilborg A, Passarelli MC, Yario TA, Tycowski KT, Steitz JA (2015) Widespread Inducible Transcription Downstream of Human Genes. *Molecular cell* **59**: 449-61
50. Nielsen M, Ard R, Leng X, Ivanov M, Kindgren P, Pelechano V, Marquardt S (2019) Transcription-driven chromatin repression of Intragenic transcription start sites. *Plos Genet* **15**: e1007969
51. Proudfoot NJ (1986) Transcriptional Interference and Termination between Duplicated Alpha-Globin Gene Constructs Suggests a Novel Mechanism for Gene-Regulation. *Nature* **322**: 562-565
52. Clough SJ, Bent AF (1998) Floral dip: a simplified method for Agrobacterium-mediated transformation of Arabidopsis thaliana. *Plant J* **16**: 735-743
53. Thodberg M, Thieffry A, Bornholdt J, Boyd M, Holmberg C, Azad A, Workman CT, Chen Y, Ekwall K, Nielsen O*, et al.* (2019) Comprehensive profiling of the fission yeast transcription start site activity during stress and media response. *Nucleic Acids Res* **47**: 1671-1691
54. Sherstnev A, Duc C, Cole C, Zacharaki V, Hornyik C, Ozsolak F, Milos PM, Barton GJ, Simpson GG (2012) Direct sequencing of Arabidopsis thaliana RNA reveals patterns of cleavage and polyadenylation. *Nat Struct Mol Biol* **19**: 845-52
55. Schurch NJ, Cole C, Sherstnev A, Song J, Duc C, Storey KG, McLean WH, Brown SJ, Simpson GG, Barton GJ (2014) Improved annotation of 3' untranslated regions and

768 complex loci by combination of strand-specific direct RNA sequencing, RNA-Seq and
769 ESTs. *PloS one* **9**: e94270
770 56. Zhang T, Marand AP, Jiang J (2016) PlantDHS: a database for DNase I hypersensitive
771 sites in plants. *Nucleic Acids Res* **44**: D1148-53
772 57. Love MI, Huber W, Anders S (2014) Moderated estimation of fold change and
773 dispersion for RNA-seq data with DESeq2. *Genome biology* **15**: 550
774 58. Anders S, Reyes A, Huber W (2012) Detecting differential usage of exons from RNA-
775 seq data. *Genome research* **22**: 2008-17
776 59. Trapnell C, Williams BA, Pertea G, Mortazavi A, Kwan G, van Baren MJ, Salzberg SL,
777 Wold BJ, Pachter L (2010) Transcript assembly and quantification by RNA-Seq reveals
778 unannotated transcripts and isoform switching during cell differentiation. *Nature*
779 *biotechnology* **28**: 511-5
780 60. Zhang R, Calixto CPG, Marquez Y, Venhuizen P, Tzioutziou NA, Guo W, Spensley M,
781 Entizne JC, Lewandowska D, Ten Have S*, et al.* (2017) A high quality Arabidopsis
782 transcriptome for accurate transcript-level analysis of alternative splicing. *Nucleic Acids*
783 *Res* **45**: 5061-5073
784 61. Trincado JL, Entizne JC, Hysenaj G, Singh B, Skalic M, Elliott DJ, Eyras E (2018)
785 SUPPA2: fast, accurate, and uncertainty-aware differential splicing analysis across
786 multiple conditions. *Genome biology* **19**: 40

787

788 Figure Legends

789 **Figure 1 Altering transcription activity of RNAPII by targeted mutagenesis in NRPB2.**

790 A. Schematic drawing of *S. cerevisiae* RNAPII transcription active center. Trigger loop is
791 shown in blue. TL-interacting Rpb2 domain is shown in beige. Proline 1018 (P1018, green)
792 and gating tyrosine 769 (Y769, red) are highlighted. The schematic drawing is based on
793 PDB: 2e2h [15].

794 B. Protein sequence alignment of RNAPII Rpb2 Y769 and P1018 regions in *S. cerevisiae* and
795 *A. thaliana*. P979S and Y732F are the yeast equivalent point mutations in *Arabidopsis*. The
796 color scheme indicates conservation from variable (blue) to conserved (red).

C. Detection of NRPB2$_{WT}$-FLAG, NRPB2$_{P979S}$-FLAG and NRPB2Y$_{732F}$-FLAG protein by western blotting in *NRPB2$_{WT}$-FLAG* Col-0, *NRPB2$_{P979S}$-FLAG* Col-0 and *NRPB2Y$_{732F}$-FLAG* Col-0 plants. Untagged NRPB2 (Col-0) was used as a negative control. Histone H3 was used as an internal control and total protein level detected by stain-free blot was used as a loading control. Quantification was done by normalizing to the loading control and anti-H3 blot based on 3 independent replicates.

D. Transmission rate of *nrpb2-2* allele in *nrpb2-2* +/- line (n=197) and *nrpb2-* +/- lines combined with homozygous *NRPB2$_{P979S}$-FLAG* +/+ (n=280), *NRPB2$_{Y732F}$-FLAG* +/+ (n=240) and *NRPB2$_{WT}$-FLAG* +/+ (n=210), respectively. Fisher´s exact test was used as a statistic test, three asterisks denote p<0.001 between samples and *n.s.* stands for not significant.

E. Image of homozygous mutant *nrpb2-2* fully complemented by *NRPB2$_{WT}$-FLAG* (top, *NRPB2$_{WT}$ +/+ nrpb2-2 -/-*) and partially complemented by *NRPB2$_{Y732F}$-FLAG* (bottom, *NRPB2$_{WT}$ +/+ nrpb2-2 -/-*). Plants were grown for 4 weeks in soil. Scale bars represent 1 cm.

Figure 2 *NRPB2$_{Y732F}$* accelerates RNAPII transcription *in vivo*.

A. Schematic drawing of the experimental design to investigate RNAPII transcription speed *in vivo*. In brief, *Arabidopsis* seedlings of *NRPB2$_{WT}$-FLAG* Col-0 and *NRPB2$_{Y732F}$-FLAG* Col-0 were grown on MS media for 12 days and then were transferred to MS liquid media for 2 days. Flagellin peptides (flagellin 22) were added into media and treated samples were collected in a 0 minute (no treatment), 2 minutes and 4 minutes time course. The nascent RNA was isolated and used for reverse transcription and qPCR analyses to reveal RNAPII accumulation at different region in genes. See Methods for technical details.

B. Nascent RNA profile of *AT5G41750*. Nascent RNA RT-qPCR assay measuring RNAPII signal at 3 positions (dark red bars: probe 1, 2 and 3) on the gene upon flagellin 22 treatment in a 0 minute, 2 minutes, 3 minutes and 4 minutes time course. Nascent RNA signal values were normalized to reference gene *ACT2*. Error bars represent SEM from 3 independent replicates. The statistical significance of differences between *NRPB2$_{Y732F}$* and *NRPB2$_{WT}$* at the same time point were assessed by the two-sided Student's t-test. n.s.

denotes not significant; * denotes p<0.05 and ** denotes p<0.01. Scale bar (black) represent 0.5 kb.

C. Nascent RNA profile of *AT4G19520*. Nascent RNA RT-qPCR assay measuring RNAPII signal at 3 positions (dark red bars: probe 1, 2 and 3) on the gene upon flagellin 22 treatment in a 0 minute, 2 minutes, 3 minutes and 4 minutes time course. Nascent RNA signal values were normalized to reference gene *ACT2*. Error bars represent SEM from 3 independent replicates. The statistical significance of differences between $NRPB2_{Y732F}$ and $NRPB2_{WT}$ at the same time point were assessed by a two-sided Student's t-test. n.s. denotes not significant; * denotes p<0.05 and ** denotes p<0.01. Scale bar (black) represents 0.5 kb.

Figure 3 Accelerated RNAPII transcription reduces promoter-proximal RNAPII stalling and enhances RNAPII activity in gene body.

A. plaNET-seq signal of RNAPII in the promoter proximal region of *AT1G70600* in $NRPB2_{WT}$ *+/+ nrpb2-2 -/-* ($NRPB2_{WT}$, blue) and $NRPB2_{Y732F}$ *+/+ nrpb2-2 -/-* ($NRPB2_{Y732F}$,red). Arrows indicate the RNAPII signal at the region of promoter-proximal stalling.

B. Metagene profile of plaNET-seq mean signal of RNAPII in a 1 Kb window centered at the +1 nucleosome in *Arabidopsis* genes (n=25474) in $NRPB2_{WT}$ *+/+ nrpb2-2 -/-* ($NRPB2_{WT}$, blue) and $NRPB2_{Y732F}$ *+/+ nrpb2-2 -/-* ($NRPB2_{Y732F}$,red). The significance of differences of plaNET-seq signal in the region from -25 bins to +25 bins around +1 nucleosome between $NRPB2_{WT}$ and $NRPB2_{Y732F}$ were assessed by a two-sided Mann-Whitney U-test, p=5.20e-10.

C. RNAPII stalling index calculated for all the genes with plaNET-Seq FPKM ≥ 10 in $NRPB2_{WT}$ *+/+ nrpb2-2 -/-* ($NRPB2_{WT}$, blue) and $NRPB2_{Y732F}$ *+/+ nrpb2-2 -/-* ($NRPB2_{Y732F}$,red) (n=6596). Medians of the stalling index are 1.891 and 1.222 for $NRPB2_{WT}$ and $NRPB2_{Y732F}$, respectively. *** denotes p-value <0.001 by Wilcoxon signed-rank test. The solid horizontal lines and box limits represent medians, lower and upper quartiles of data values in each group. The upper and lower whiskers extend to the largest or smallest value, respectively, no further than 1.5 * IQR from the relevant quartile.

D. Metagene profile of plaNET-seq mean signal over whole genes (length from 0.5 Kb to 5 Kb, scaled to 500 bins, n=27042) in *NRPB2*$_{WT}$ *+/+ nrpb2-2 -/-* (*NRPB2*$_{WT}$, blue) and *NRPB2*$_{Y732F}$ *+/+ nrpb2-2 -/-* (*NRPB2*$_{Y732F}$,red).

E. Metagene profile of plaNET-seq mean signal of RNAPII in exons (length from 50 bp to 300 bp, scaled to 100 bins, n=73925) in *NRPB2*$_{WT}$ *+/+ nrpb2-2 -/-* (*NRPB2*$_{WT}$, blue) and *NRPB2*$_{Y732F}$ *+/+ nrpb2-2 -/-* (*NRPB2*$_{Y732F}$,red). Pink dashed line rectangle illustrates the amplitude of differences between the minimum and the maximum of RNAPII signal across the exons. A two-sided Mann-Whitney U-test was used to assess the plaNET-seq signal of *NRPB2*$_{WT}$ (blue) and *NRPB2*$_{Y732F}$ (red) in exons, p<1e-16.

F. Metagene profile of plaNET-seq mean signal of RNAPII in introns (50 bp to 300 bp, scaled to 100 bins, n=102260) in *NRPB2*$_{WT}$ *+/+ nrpb2-2 -/-* (*NRPB2*$_{WT}$, blue) and *NRPB2*$_{Y732F}$ *+/+ nrpb2-2 -/-* (*NRPB2*$_{Y732F}$,red). A two-sided Mann-Whitney U-test was used to assess the plaNET-seq signal of *NRPB2*$_{WT}$ (blue) and *NRPB2*$_{Y732F}$ (red) in introns, p<1e-16.

Figure 4 Analysis of alternative splicing in *NRPB2*$_{WT}$ and *NRPB2*$_{Y732F}$ mutant.

A. A schematic illustration of the co-transcriptional RNAPII-spliceosome complex. plaNET-seq mainly detects splicing intermediates corresponding to 5' splicing site (5'SS) co-purified with engaged RNAPII complex.

B. Bar charts showing the fractions of 3' and 5' splicing intermediate reads from plaNET-seq in *NRPB2*$_{WT}$ *+/+ nrpb2-2 -/-* (*NRPB2*$_{WT}$, blue) and *NRPB2*$_{Y732F}$ *+/+ nrpb2-2 -/-* (*NRPB2*$_{Y732F}$,red).

C. Genome browser snapshots illustrating enhanced intron splicing in *NRPB2*$_{Y732F}$ *+/+ nrpb2-2 -/-* (*NRPB2*$_{Y732F}$, red) compared to *NRPB2*$_{WT}$ *+/+ nrpb2-2 -/-* (*NRPB2*$_{WT}$,blue). Scale bars denote 0.5 Kb.

D. The fraction of RNA-seq intronic reads calculated for all genes (n=24912) in *NRPB2*$_{WT}$ *+/+ nrpb2-2 -/-* and *NRPB2*$_{Y732F}$ *+/+ nrpb2-2 -/-*. Two-sided Mann-Whitney U test: **** denotes p-value<2.2e-16. The solid horizontal lines and box limits represent medians, lower and upper quartiles of data values in each group. The upper and lower whiskers extend to the largest or smallest value, respectively, no further than 1.5 * IQR from the relevant quartile.

E. Differentially expressed (DE) exons and introns in *NRPB2*$_{Y732F}$ *+/+ nrpb2-2 -/-* compared to *NRPB2*$_{WT}$ *+/+ nrpb2-2 -/-* based on RNA-seq results. Numbers of DE exons and introns were shown in plot.

F. Quantification (log fold change of FPKM from RNA-seq) of differentially expressed (DE) exons and non-DE exons in *NRPB2*$_{Y732F}$ *+/+ nrpb2-2 -/-* compared to *NRPB2*$_{WT}$ *+/+ nrpb2-2 -/-*. ** denotes p-value <0.01 by Wilcoxon signed-rank test. The solid horizontal lines and box limits represent medians, lower and upper quartiles of data values in each group. The upper and lower whiskers extend to the largest or smallest value, respectively, no further than 1.5 * IQR from the relevant quartile.

G. Genome browser snapshots illustrating enhanced exon skipping in *NRPB2*$_{Y732F}$ *+/+ nrpb2-2 -/-* (*NRPB2*$_{Y732F}$, red) compared to *NRPB2*$_{WT}$ *+/+ nrpb2-2 -/-* (*NRPB2*$_{WT}$,blue). Scale bars denote 0.5 Kb.

H. Quantification (log fold change of FPKM from RNA-seq) of differentially expressed (DE) introns and non-DE exons in *NRPB2*$_{Y732F}$ *+/+ nrpb2-2 -/-* compared to *NRPB2*$_{WT}$ *+/+ nrpb2-2 -/-*. **** denotes p-value <0.0001 by Wilcoxon signed-rank test. The solid horizontal lines and box limits represent medians, lower and upper quartiles of data values in each group. The upper and lower whiskers extend to the largest or smallest value, respectively, no further than 1.5 * IQR from the relevant quartile.

Figure 5 Accelerated transcription reduces RNAPII stalling at 3' gene ends and enhances transcriptional read-through downstream of PAS.

A. plaNET-seq signal of RNAPII at 3' end of *AT2G21410* in *NRPB2*$_{WT}$ *+/+ nrpb2-2 -/-* (*NRPB2*$_{WT}$, blue) and *NRPB2*$_{Y732F}$ *+/+ nrpb2-2 -/-* (*NRPB2*$_{Y732F}$,red). Arrows indicate the RNAPII signal peaks at PAS stalling region.

B. Metagene profile of plaNET-seq mean signal of RNAPII in a 1 kb window centered at PAS (n=24448) in *NRPB2*$_{WT}$ *+/+ nrpb2-2 -/-* (*NRPB2*$_{WT}$, blue) and *NRPB2*$_{Y732F}$ *+/+ nrpb2-2 -/-* (*NRPB2*$_{Y732F}$,red). The significance of differences of plaNET-seq signal in the region from PAS to +100 bins between *NRPB2*$_{WT}$ and *NRPB2*$_{Y732F}$ were assessed by Two-sided Mann-Whitney U-test, p = 1.53e-06.

C. Histogram of transcriptional read-through length (nt) from PAS of protein-coding gene (plaNET-seq FPKM>5, n=9316) in *NRPB2*$_{WT}$ +/+ *nrpb2-2 -/-* (*NRPB2*$_{WT}$, blue) and *NRPB2*$_{Y732F}$ +/+ *nrpb2-2 -/-* (*NRPB2*$_{Y732F}$,red).

D. Box plot shows the RNAPII transcriptional read-through length from PAS of protein-coding genes (plaNET-seq FPKM>5 n=9316) called based on statistic model (see Methods) in *NRPB2*$_{WT}$ +/+ *nrpb2-2 -/-* (*NRPB2*$_{WT}$, blue) and *NRPB2*$_{Y732F}$ +/+ *nrpb2-2 -/-* (*NRPB2*$_{Y732F}$,red). Median of read-through length in *NRPB2*$_{WT}$ and *NRPB2*$_{Y732F}$ mutant are 534 nt and 649 nt. Two-sided Mann-Whitney U-test: *** denotes p = 9.9e-62. The solid horizontal lines and box limits represent medians, lower and upper quartiles of data values in each group. The upper and lower whiskers extend to the largest or smallest value, respectively, no further than 1.5 * IQR from the relevant quartile.

E. Metagene plot of RNAPII signal by plaNET-seq anchored at both PAS of upstream genes and TSS of downstream genes for tandemly oriented genes (n=5753) in *NRPB2*$_{WT}$ +/+ *nrpb2-2 -/-* (*NRPB2*$_{WT}$, blue) and *NRPB2*$_{Y732F}$ +/+ *nrpb2-2 -/-* (*NRPB2*$_{Y732F}$,red). Red arrow denotes the direction of transcriptional read-through. Pink dashed line rectangle indicates the region corresponding to the second half of PAS-TSS gaps along 5' to 3' direction.

F. Metagene plot of RNAPII signal by plaNET-seq anchored at PASs of both upstream genes and downstream genes for gene pairs located in "tail to tail" orientation (n=1384) in *NRPB2*$_{WT}$ +/+ *nrpb2-2 -/-* (*NRPB2*$_{WT}$, blue) and *NRPB2*$_{Y732F}$ +/+ *nrpb2-2 -/-* (*NRPB2*$_{Y732F}$,red). Red arrows denote the directions of transcriptional read-through from both PASs. Pink dashed line rectangles indicate the region corresponding to the second half of PAS-TSS gaps along 5' to 3' direction.

Figure 6 Cartoon summarizing the effect of *NRPB2*$_{Y732F}$ on RNAPII genomic stalling and transcription read-through.

A. A schematic illustrating the effect of transcription speed on RNAPII stalling at promoter proximal regions. Accelerated RNAPII is prone to move out of stalling regions (centered at the position of the first nucleosome) at 5' end of genes, resulting in reduced promoter proximal stalling peaks in RNAPII profile by plaNET-seq.

B. A schematic illustration showing that accelerated RNAPII tends to evade from RNAPII stalling near gene poly-(A) sites (PAS). This leads to less efficient transcription termination and extended transcription read-through, reflected by the absence of RNAPII signal peaks downstream of PAS and elevated signal downstream of PAS stalling region by plaNET-seq.

Figure EV1 Generation and characterization of *Arabidopsis* NRPB2 point mutations (related to Figure 1)

A. Schematic overview of a work flow to generate $NRPB2_{WT}$ +/+ *nrpb2-2 -/-*, $NRPB2_{Y732F}$ +/+ *nrpb2-2 -/-* and $NRPB2_{P979S}$ *+/+ nrpb2-2 +/- Arabidopsis*. First, constructs harboring $NRPB2_{WT}$ (blue), $NRPB2_{Y732F}$ (red) and $NRPB2_{P979S}$ (green) transgene expression cassette were transformed into wildtype (Col-0) *Arabidopsis* via agrobacterium-mediated transformation; T3 transformant plants with homozygous transgenes are crossed with *nrpb2-2 +/-* (grey) heterozygous *Arabidopsis*, then plants positive for both transgenes and *nrpb2-2* allele were selected for propagation into F3 generation to screen for homozygous double mutants of transgene and *nrpb2-2*.

B. Phenotype of *Arabidopsis* siliques of wild type (Col-0), $NRPB2_{Y979S}$ *+/+* Col-0 and $NRPB2_{Y979S}$ *nrpb2-2 +/-* plants. Scale bars represent 10 mm.

C. Silique length of wild type (Col-0), $NRPB2_{Y979S}$ Col-0 and $NRPB2_{Y979S}$ +/+ *nrpb2-2 +/-* plants (n>20 for each genotype). Two-sided Student's T test was used for statistic test, *** denotes p<0.001. The solid horizontal lines and box limits represent medians, lower and upper quartiles of data values in each group. The upper and lower whiskers extend to the largest or smallest value, respectively, no further than 1.5 * IQR from the relevant quartile.

D. Opened siliques from wild type (Col-0), $NRPB2_{Y979S}$ +/+ Col-0 and $NRPB2_{Y979S}$ +/+ *nrpb2-2 +/-* plants. Red arrows indicate aborted ovules.

E. Phenotype of alternative transformation events to lines presented in Figure 1E. Homozygous mutant *nrpb2-2* was fully complemented by *NRPB2-FLAG* (top) and partially complemented by $NRPB2_{Y732F}$*-FLAG* (bottom). Plants were grown for 4 weeks in soil. Scale bars represent 1 cm.

F. Relative expression level of *PR1*, *PR2* and *PR5* in $NRPB2_{WT}$ +/+ *nrpb2-2* -/- and $NRPB2_{Y732F}$ +/+ *nrpb2-2* -/- by RT-qPCR. Error bars represent SEM from 3 independent replicates. ** denotes p<0.01 by two-sided Student's T test.

Figure EV2 Molecular and phenotypic characterization of the *rpb2-Y769F* mutation in budding yeast and *Arabidopsis* equivalent $NRPB2_{Y732F}$ (related to Figure 2)

A. Differential sensitivity of various budding yeast *rpb2* mutants towards Mn^{2+} and MPA in SC-Leu media.

B. Primer extension analyses for *ADH1* transcription start site usage in *rpb2* mutants in budding yeast.

C. Genetic interaction between *rpb2-Y769F* and *Rpb1* TL mutations. Growth was assayed at day 1 and day 5. Ability to grow on SC-Leu+5FOA indicates that *rpb2-Y769F* counteracts *Rpb1* TL mutations. Red box indicates the phenotype of *rpb2-Y769F* crossed with *Rpb1* TL mutations.

D. A work flow of immunoprecipitation (IP) of FLAG-tagged NRPB2 protein by anti-FLAG followed by nascent RNA isolation, RT-qPCR analyses and plaNET-seq (left). Western blotting (right) of $NRPB2_{WT}$-FLAG and $NRPB2_{Y732F}$-FLAG as IP input (input), after IP (un-bound) and after elution by FLAG peptides (eluted). Upper panel shows representative anti-FLAG blots. Lower panel shows total proteins as loading control for indicated fractions.

E. Nascent RNA profile of *AT5G41740*. Nascent RNA RT-qPCR assay measuring RNAPII signal at 3 positions (dark red bars: probe 1, 2 and 3) on gene upon flagellin 22 treatment in a 0 minute, 2 minutes, 3 minutes and 4 minutes time course. Nascent RNA signal values were normalized to reference gene *ACT2*. Error bars represent SEM from 3 independent replicates. The statistical significance of differences between $NRPB2_{Y732F}$ and $NRPB2_{WT}$ at the same time point were assessed by two-sided Student's t-test. n.s. denotes not significant; * denotes p<0.05 and ** denotes p<0.01. Scale bar (black) represent 0.5 kb.

Figure EV3 Genome-wide effects of $NRPB2_{Y732F}$ on nascent RNAPII transcription by plaNET-seq compared to $NRPB2_{WT}$ (related to Figure 3)

A. Scatterplot showing the biological reproducibility of plaNET-Seq experiment in *NRPB2*$_{WT}$ *+/+ nrpb2-2 -/-*. TPM-normalized plaNET-Seq signal was summarized within 10 bp bins genome-wide. Pearson R=0.987.

B. Scatterplot showing the biological reproducibility of plaNET-Seq experiment in *NRPB2*$_{Y732F}$ *+/+ nrpb2-2 -/-*. TPM-normalized plaNET-Seq signal was summarized within 10 bp bins genome-wide. Pearson R=0.987.

C. Metagene profile of plaNET-seq mean signal of RNAPII in a 1 Kb window centered at the TSS of *Arabidopsis* genes (n=24862) in *NRPB2*$_{WT}$ (blue) and *NRPB2*$_{Y732F}$ (red).

D. plaNET-seq signal of RNAPII across the whole *AT2G19830* gene in *NRPB2*$_{WT}$ (blue) and *NRPB2*$_{Y732F}$ (red). Arrows indicate the elevated nascent RNAPII signal in the gene body.

E. Metagene profile of plaNET-seq mean signal of RNAPII in exons (50 bp to 100 bp, scaled to 100 bins, n=31202) in *NRPB2*$_{WT}$ *+/+ nrpb2-2 -/-* (*NRPB2*$_{WT}$, blue) and *NRPB2*$_{Y732F}$ *+/+ nrpb2-2 -/-* (*NRPB2*$_{Y732F}$,red).

F. Metagene profile of plaNET-seq mean signal of RNAPII in exons (100 bp to 200 bp, scaled to 100 bins, n=33600) in *NRPB2*$_{WT}$ *+/+ nrpb2-2 -/-* (*NRPB2*$_{WT}$, blue) and *NRPB2*$_{Y732F}$ *+/+ nrpb2-2 -/-* (*NRPB2*$_{Y732F}$,red).

G. Metagene profile of plaNET-seq mean signal of RNAPII in exons (200 bp to 300 bp, scaled to 100 bins, n=9795) in *NRPB2*$_{WT}$ *+/+ nrpb2-2 -/-* (*NRPB2*$_{WT}$, blue) and *NRPB2*$_{Y732F}$ *+/+ nrpb2-2 -/-* (*NRPB2*$_{Y732F}$,red).

H. Metagene profile of plaNET-seq mean signal of RNAPII in introns (50 bp to 100 bp, scaled to 100 bins, n=58050) in *NRPB2*$_{WT}$ *+/+ nrpb2-2 -/-* (*NRPB2*$_{WT}$, blue) and *NRPB2*$_{Y732F}$ *+/+ nrpb2-2 -/-* (*NRPB2*$_{Y732F}$,red).

I. Metagene profile of plaNET-seq mean signal of RNAPII in introns (100 bp to 200 bp, scaled to 100 bins, n=34213) in *NRPB2*$_{WT}$ *+/+ nrpb2-2 -/-* (*NRPB2*$_{WT}$, blue) and *NRPB2*$_{Y732F}$ *+/+ nrpb2-2 -/-* (*NRPB2*$_{Y732F}$,red).

J. Metagene profile of plaNET-seq mean signal of RNAPII in introns (200 bp to 300 bp, scaled to 100 bins, n=128) in *NRPB2*$_{WT}$ *+/+ nrpb2-2 -/-* (*NRPB2*$_{WT}$, blue) and *NRPB2*$_{Y732F}$ *+/+ nrpb2-2 -/-* (*NRPB2*$_{Y732F}$,red).

K. Metagene profile of plaNET-seq mean signal of RNAPII in constitutive exons (n=75136) in *NRPB2*$_{WT}$ *+/+ nrpb2-2 -/-* (*NRPB2*$_{WT}$, blue) and *NRPB2*$_{Y732F}$ *+/+ nrpb2-2 -/-* (*NRPB2*$_{Y732F}$,red).

L. Metagene profile of plaNET-seq mean signal of RNAPII in alternative exons (n=724) in *NRPB2*$_{WT}$ *+/+ nrpb2-2 -/-* (*NRPB2*$_{WT}$, blue) and *NRPB2*$_{Y732F}$ *+/+ nrpb2-2 -/-* (*NRPB2*$_{Y732F}$,red).

M. Metagene profile of plaNET-seq mean signal of RNAPII in constitutive exons (n=97358) in *NRPB2*$_{WT}$ *+/+ nrpb2-2 -/-* (*NRPB2*$_{WT}$, blue) and *NRPB2*$_{Y732F}$ *+/+ nrpb2-2 -/-* (*NRPB2*$_{Y732F}$,red).

N. Metagene profile of plaNET-seq mean signal of RNAPII in alternative exons (n=5306) in *NRPB2*$_{WT}$ *+/+ nrpb2-2 -/-* (*NRPB2*$_{WT}$, blue) and *NRPB2*$_{Y732F}$ *+/+ nrpb2-2 -/-* (*NRPB2*$_{Y732F}$,red).

Figure EV4 Genome-wide effects of *NRPB2*$_{Y732F}$ on gene expression by RNA-seq compared to *NRPB2*$_{WT}$ (related to Figure 4)

A. Reproducibility of RNA-seq data demonstrated by clustered heatmap of Euclidean distances between two independent replicates of RNA-seq in both *NRPB2*$_{WT}$ *+/+ nrpb2-2 -/-* and *NRPB2*$_{Y732F}$ *+/+ nrpb2-2 -/-.* Darker blue stands for higher reproducibility and lighter blue represents low reproducibility.

B. Illustration of constitutive splicing site (SS), alternative 5' splicing site (SS) and alternative 3' splicing site (SS).

C. Differentially regulated alternative 5'SS and 3'SS in *NRPB2*$_{Y732F}$ *+/+ nrpb2-2 -/-* compared to *NRPB2*$_{WT}$ *+/+ nrpb2-2 -/-* based on RNA-seq results. Numbers of up- and down-regulated SS were shown in plot.

D. Quantification (the changes of present splicing inclusion, dPSI) of differentially regulated alternative 3'SS exons and non-DE exons in *NRPB2*$_{Y732F}$ *+/+ nrpb2-2 -/-* compared to *NRPB2*$_{WT}$ *+/+ nrpb2-2 -/-*. dPSI>0 and dPSI<0 suggest upstream and downstream shift of alternative 5'SS, respectively. **** denotes p-value <0.0001 by Wilcoxon signed-rank test. The solid horizontal lines and box limits represent medians, lower and upper quartiles of data values in each group. The upper and lower whiskers extend to the largest or smallest value, respectively, no further than 1.5 * IQR from the relevant quartile.

E. Quantification (the changes of present splicing inclusion, dPSI) of differentially regulated alternative 5'SS exons and non-DE exons in *NRPB2*$_{Y732F}$ *+/+ nrpb2-2 -/-* compared to *NRPB2*$_{WT}$ *+/+ nrpb2-2 -/-*. dPSI>0 and dPSI<0 suggest downstream and upstream shift of alternative 5'SS, respectively. ** denotes p-value <0.01 by Wilcoxon signed-rank test. The solid horizontal lines and box limits represent medians, lower and upper quartiles of data values in each group. The upper and lower whiskers extend to the largest or smallest value, respectively, no further than 1.5 * IQR from the relevant quartile.

Figure EV5 Quantification of read-through transcription in *NRPB2*$_{Y732F}$ compared to *NRPB2*$_{WT}$ (related to Figure 5)

A. Box plot showing the comparison of plaNET-seq signal of *NRPB2*$_{WT}$ (blue) and *NRPB2*$_{Y732F}$ (red) in the region corresponding to the second half of PAS-TSS gaps (n=5753) between tandemly oriented genes. Mann-Whitney test, **** denotes p=1.70e-43. The solid horizontal lines and box limits represent medians, lower and upper quartiles of data values in each group. The upper and lower whiskers extend to the largest or smallest value, respectively, no further than 1.5 * IQR from the relevant quartile.

B. Box plot showing the comparison of plaNET-seq signal of *NRPB2*$_{WT}$ (blue) and *NRPB2*$_{Y732F}$ (red) in the region corresponding to the second half of PAS-PAS gaps (n=1384) between genes located in "tail to tail" orientation. Mann-Whitney test, **** denotes p=7.10e-14. The solid horizontal lines and box limits represent medians, lower and upper quartiles of data values in each group. The upper and lower whiskers extend to the largest or smallest value, respectively, no further than 1.5 * IQR from the relevant quartile.

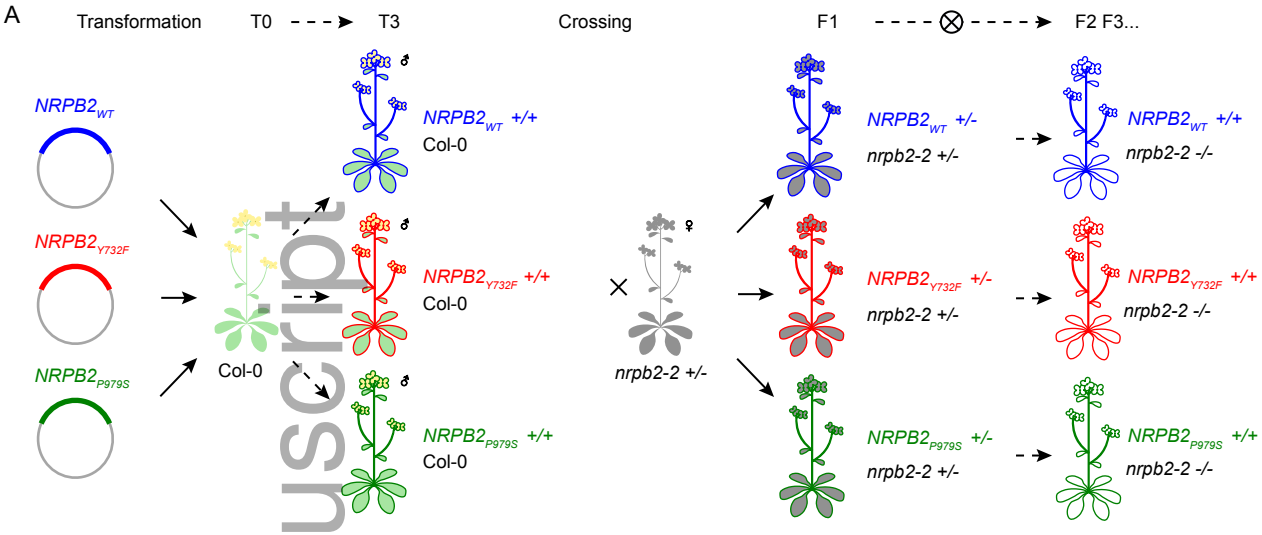

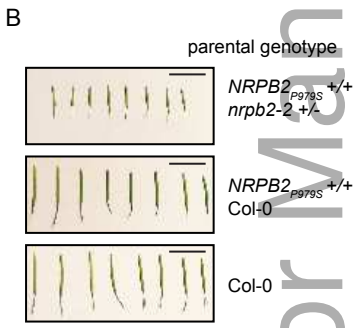

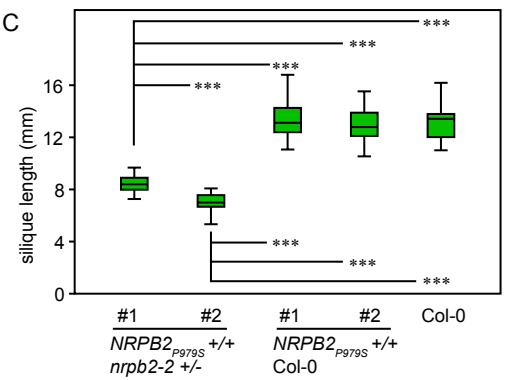

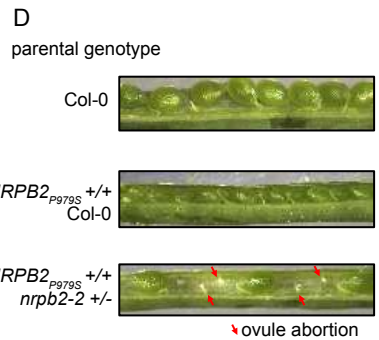

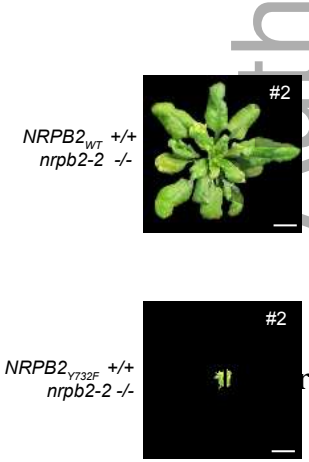

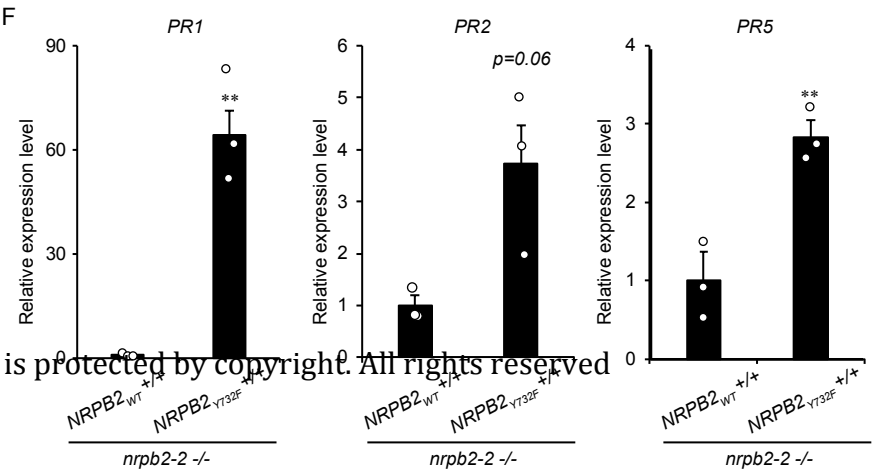

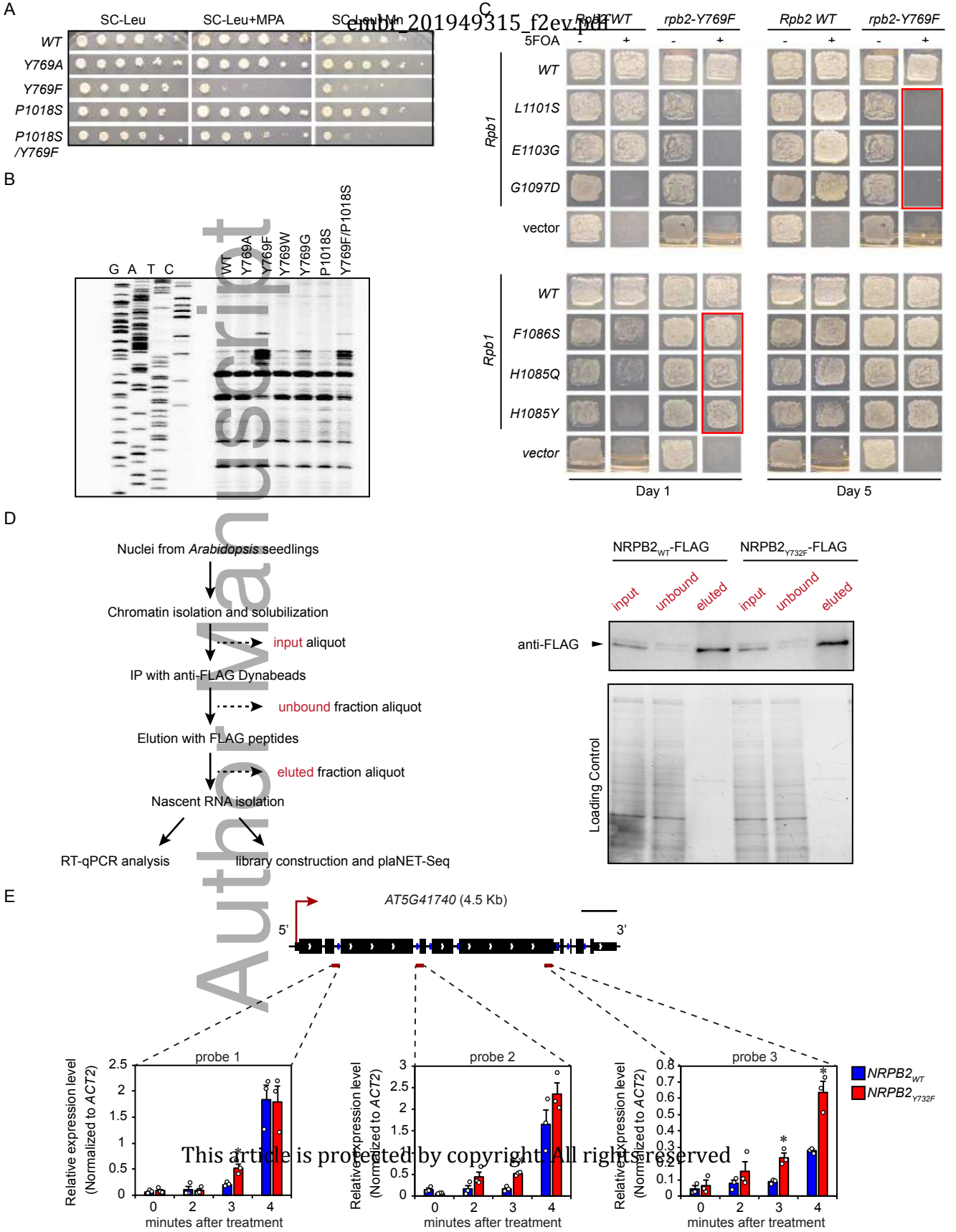

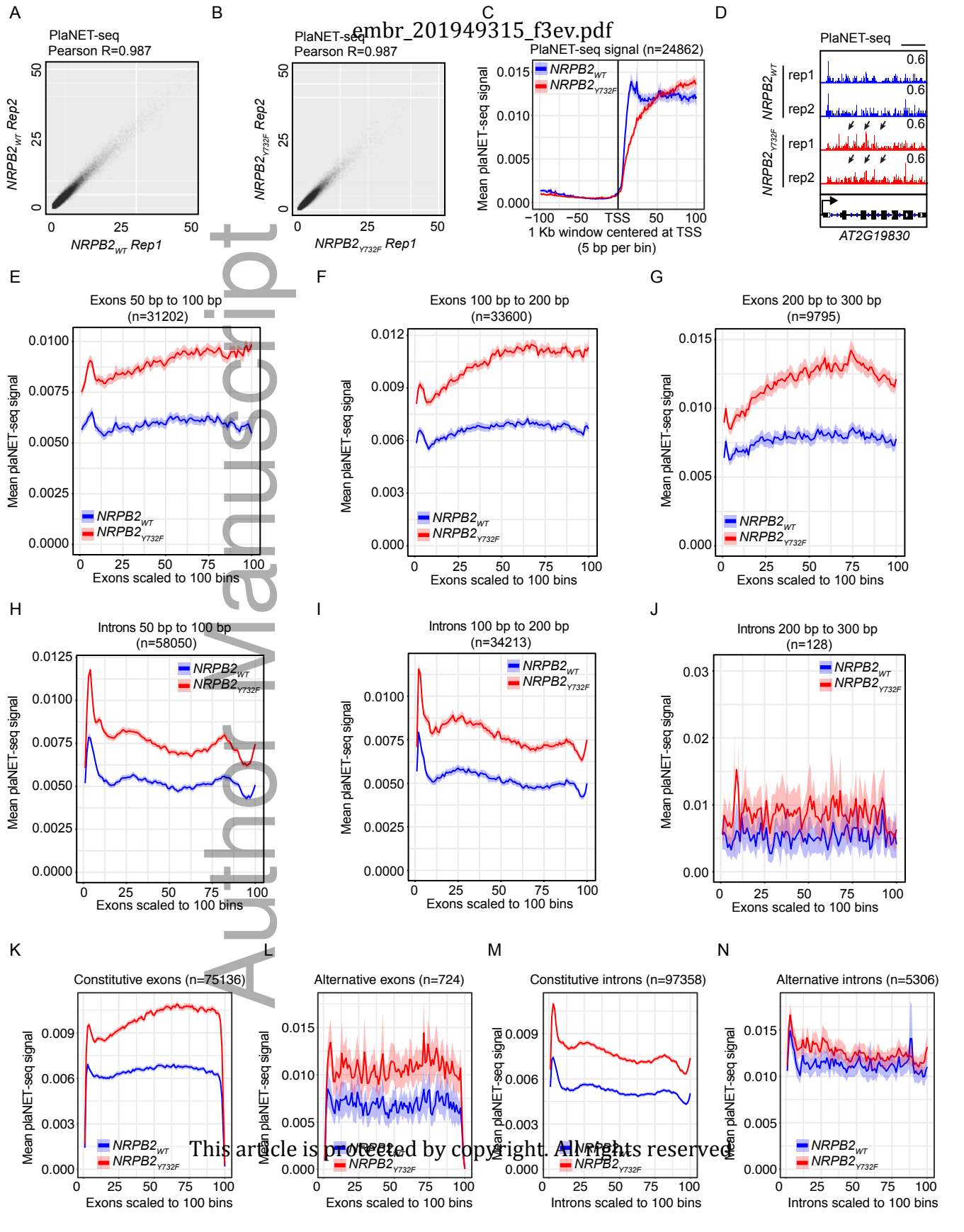

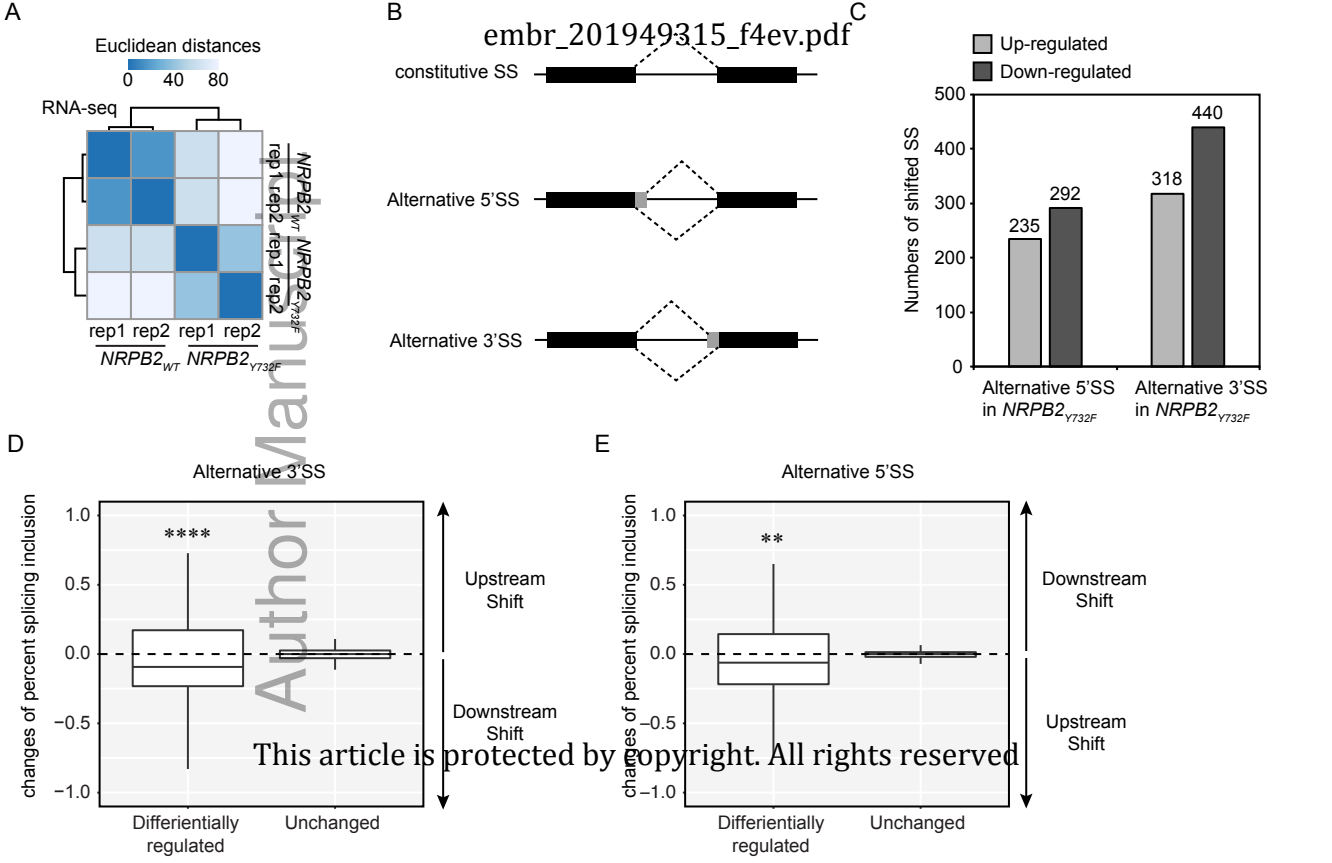

A